Global Biogeochemical Cycles®

RESEARCH ARTICLE
10.1029/2022GB007528

Dissolved, Labile, and Total Particulate Trace Metal Dynamics on the Northeast Greenland Shelf

Xue-Gang Chen[1,2], Stephan Krisch[2,3], Ali Al-Hashem[2], Mark James Hopwood[4], Michiel M. Rutgers van der Loeff[5], Oliver Huhn[6], Pablo Lodeiro[7], Tim Steffens[2], and Eric P. Achterberg[2]

[1]Ocean College, Zhejiang University, Zhoushan, China, [2]GEOMAR Helmholtz Centre for Ocean Research Kiel, Kiel, Germany, [3]Now at Bundesanstalt für Gewässerkunde, Koblenz, Germany, [4]Department of Ocean Science and Engineering, Southern University of Science and Technology, Shenzhen, China, [5]Alfred Wegener Institute, Helmholtz Centre for Polar and Marine Research, Bremerhaven, Germany, [6]IUP – Institute of Environmental Physics, University of Bremen, Bremen, Germany, [7]Department of Chemistry, Universitat de Lleida – AGROTECNIO-CERCA Center, Lleida, Spain

Abstract We present high-resolution profiles of dissolved, labile, and total particulate trace metals (TMs) on the Northeast Greenland shelf from GEOTRACES cruise GN05 in August 2016. Combined with radium isotopes, stable oxygen isotopes, and noble gas measurements, elemental distributions suggest that TM dynamics were mainly regulated by the mixing between North Atlantic-derived Intermediate Water, enriched in labile particulate TMs (LpTMs), and Arctic surface waters, enriched in Siberian shelf-derived dissolved TMs (dTMs; Co, Cu, Fe, Mn, and Ni) carried by the Transpolar Drift. These two distinct sources were delineated by salinity-dependent variations of dTM and LpTM concentrations and the proportion of dTMs relative to the total dissolved and labile particulate ratios. Locally produced meltwater from the Nioghalvfjerdsbræ (79NG) glacier cavity, distinguished from other freshwater sources using helium excess, contributed a large pool of dTMs to the shelf inventory. Localized peaks in labile and total particulate Cd, Co, Fe, Mn, Ni, Cu, Al, V, and Ti in the cavity outflow, however, were not directly contributed by submarine melting. Instead, these particulate TMs were mainly supplied by the re-suspension of cavity sediment particles. Currently, Arctic Ocean outflows are the most important source of dFe, dCu, and dNi on the shelf, while LpTMs and up to 60% of dMn and dCo are mainly supplied by subglacial discharge from the 79NG cavity. Therefore, changes in the cavity-overturning dynamics of 79NG induced by glacial retreat, and alterations in the transport of Siberian shelf-derived materials with the Transport Drift may shift the shelf dTM-LpTM stoichiometry in the future.

Plain Language Summary Trace metals (TMs) including cobalt (Co), iron (Fe), manganese (Mn), copper (Cu), and nickel (Ni) are essential micronutrients for marine productivity. The Northeast Greenland shelf is a climatically sensitive region, influenced by both outflowing Arctic waters and local glacier melting. We lack knowledge on how these Arctic surface waters affect TM dynamics on the Greenland shelf and how climatic shifts may influence TM dynamics. Here, we distinguish local submarine meltwater from Arctic surface waters using distinct tracers; noble gases and radium isotopes. We show that the TM dynamics on the shelf are largely controlled by the intrusion of Arctic surface waters which creates a near-surface plume of dissolved and labile particulate TMs. Conversely, submarine meltwater creates a subsurface plume enriched in dissolved TMs but depleted in particulate TMs, which is exported from underneath a floating ice tongue. In the future, increasing Arctic river discharge and local glacial melting may both significantly change shelf micronutrient ratios demonstrating downstream impacts of a changing cryosphere on marine biogeochemical cycles.

Key Points:

- The overall dissolved and particulate trace metal (TM) dynamics were mainly regulated by the mixing with Arctic surface waters
- Resuspension of cavity sediments is a major localized source of labile and total particulate Cd, Co, Fe, Mn, Ni, Cu, Al, V, and Ti
- Whilst dissolved and particulate TMs are mostly coupled on the Greenland shelf, cavity outflow decouples both phases

Supporting Information:

Supporting Information may be found in the online version of this article.

Correspondence to:

X.-G. Chen and E. P. Achterberg,
xchen@geomar.de;
eachterberg@geomar.de

Citation:

Chen, X.-G., Krisch, S., Al-Hashem, A., Hopwood, M. J., Rutgers van der Loeff, M. M., Huhn, O., et al. (2022). Dissolved, labile, and total particulate trace metal dynamics on the Northeast Greenland shelf. *Global Biogeochemical Cycles*, *36*, e2022GB007528. https://doi.org/10.1029/2022GB007528

Received 18 JUL 2022
Accepted 20 NOV 2022

Author Contributions:

Conceptualization: Xue-Gang Chen, Eric P. Achterberg
Formal analysis: Xue-Gang Chen, Stephan Krisch, Ali Al-Hashem, Michiel M. Rutgers van der Loeff, Oliver Huhn, Tim Steffens
Funding acquisition: Eric P. Achterberg
Investigation: Xue-Gang Chen, Stephan Krisch, Ali Al-Hashem, Michiel M. Rutgers van der Loeff, Oliver Huhn, Pablo Lodeiro, Tim Steffens, Eric P. Achterberg

1. Introduction

In addition to macronutrients (fixed nitrogen (NO_3 + NO_2), phosphate (PO_4), and silicic acid), trace metals (TMs) including iron (Fe), cobalt (Co), nickel (Ni), copper (Cu), manganese (Mn), and cadmium (Cd) have attracted research interest due to their roles in marine primary productivity (Morel & Price, 2003; Twining & Baines, 2013). Because the supply of bio-essential TMs is in large parts of the global ocean insufficient to fully meet phytoplankton growth requirements (C. M. Moore et al., 2013), short-term growth of phytoplankton communities is often TM limited or co-limited (e.g., Behrenfeld & Kolber, 1999; Browning et al., 2021, 2022; Panzeca et al., 2008; Price & Morel, 1991; Xu & Morel, 2013). Phytoplankton primarily assimilate TMs from dissolved

Methodology: Xue-Gang Chen, Ali Al-Hashem, Mark James Hopwood, Pablo Lodeiro
Resources: Eric P. Achterberg
Visualization: Xue-Gang Chen
Writing – original draft: Xue-Gang Chen, Mark James Hopwood, Eric P. Achterberg
Writing – review & editing: Xue-Gang Chen, Stephan Krisch, Mark James Hopwood, Michiel M. Rutgers van der Loeff, Oliver Huhn, Pablo Lodeiro, Eric P. Achterberg

phases (dissolved TMs [dTMs]) (Morel & Price, 2003) yet, particularly in shelf seas, a large fraction of the TM inventory is found in particulate phases (particulate TMs [pTMs]; specifically labile pTMs [LpTMs] and total pTMs [TpTMs]), which may play an important role in moderating dTM availability. LpTMs, a fraction which includes cellular material, can be solubilized and become accessible to phytoplankton (Baeyens et al., 2011; Twining et al., 2015) and may buffer the size of the dissolved pool for elements such as Fe which exhibit rapid exchange between dissolved and particulate phases (Homoky et al., 2012; Lippiatt et al., 2010).

Whilst internal cycling regulates the bioavailability of TMs, TM concentrations are also influenced by external sources, for example, rivers and atmospheric deposition. Freshwater and the associated sediment load is especially important as a driver of TM distributions in the Arctic (Charette et al., 2020; Guieu et al., 1996; Gerringa et al., 2021). The Arctic Ocean receives ∼11% of global riverine input despite accounting for only 1% of the global ocean volume, and is similarly disproportionately affected by shelf sediment interactions (Aagaard & Carmack, 1989). Organic material and TMs (e.g., shelf-derived Fe $1.0 \pm 0.5 \times 10^8$ and Cu $2.0 \pm 1.0 \times 10^8$ mol yr^{-1}; Charette et al., 2020) are continuously delivered from large rivers (such as the Ob, Lena, and Yenisey) into the Arctic Ocean (Dai & Martin, 1995; Gordeev, 2000; Guieu et al., 1996). Whilst nitrate is thought to be the main limiting nutrient for phytoplankton growth across most of the Arctic, Arctic surface waters may function as a source of TMs to other ocean basins, particularly the high latitude North Atlantic (Charette et al., 2020; Krisch, Hopwood, et al., 2022). After substantial estuarine removal (J. Zhang, 1995; Sholkovitz, 1978) followed by biological drawdown and scavenging during lateral transportation, TMs originating from the Siberian shelf are carried into the North Atlantic Ocean via the Transpolar Drift (TPD) through the Fram Strait (Charette et al., 2020; Krisch, Hopwood, et al., 2022). This Arctic Ocean outflow, characterized by low salinity and high dTM content, occupies the surface water layer on the outer parts of the Northeast (NE) Greenland shelf and may influence primary production in this region (Krisch et al., 2020; Tuerena et al., 2021), with potential consequences for TM availability in the downstream East Greenland Current (EGC; Krisch, Hopwood, et al., 2022; Tonnard et al., 2020).

In addition to a strong influence of Arctic outflow, the NE Greenland shelf receives large inputs from glaciers including Nioghalvfjerdsbræ (79NG) and Zachariæ Isstrøm (ZI), with drainage areas of ∼200,000 km^2 which represents about 12% of the Greenland Ice Sheet by area (An et al., 2021; Rignot & Mouginot, 2012). Due to ongoing global warming and the exposure of the Greenlandic ice shelves to inflowing warm Atlantic water, since 2012 ZI has lost about 98% of its floating ice tongue (Mouginot et al., 2015). Although 79NG is relatively stable by comparison, the floating ice tongue of 79NG is also retreating (Mayer et al., 2018) and Spalte Glacier, a side-branch of the ice tongue formerly draining into Dijmphna Sund, disintegrated entirely in July 2020 (NASA, 2022). The 79NG hosts the largest present day floating ice tongue around the entire coast of Greenland (Mayer et al., 2000; Mouginot et al., 2015; Schaffer et al., 2020). The glacial cavity underneath the floating tongue is potentially an "incubator," moderating the outflowing TM signature onto the NE Greenland shelf by providing a sufficiently long period of time to establish a thermodynamic equilibrium between dissolved and particulate phases entering the cavity from ice melt, subglacial discharge, saline inflow, and sediment resuspension (Krisch, Hopwood, et al., 2021). The isolation of glacier cavity from biological processes also helps better understanding the geochemical cycling of TMs in Arctic fjord systems. Whilst the cavity itself is inaccessible to ship-based observations, and all inferences primarily refer to a comparison of inflowing and outflowing AIW composition, there is a potential to use tracers to distinguish different processes affecting TM dynamics on the NE Greenland shelf. For instance, different freshwater sources (Arctic rivers, submarine meltwater, surface runoff) can be distinguished by considering Helium (He) and Neon (Ne) (Beaird et al., 2015; Huhn, Rhein, Kanzow, et al., 2021; Loose & Jenkins, 2014) and stable oxygen isotopes ($\delta^{18}O$) (Tiwari et al., 2018). Local sedimentary inputs and Arctic river discharge can be further traced by radium (Ra) isotopes as Arctic surface waters show both strongly elevated $^{228}Ra/^{226}Ra$ ratios and reduced salinity and $\delta^{18}O$ values (Charette et al., 2016; Kipp et al., 2018; Rutgers van der Loeff et al., 2012). Elements such as aluminum (Al), vanadium (V), and titanium (Ti), may also be insightful for tracing lithogenic particle inputs and distinguishing different regional TM sources and sinks (e.g., Barrett et al., 2018; Menzel Barraqueta et al., 2018).

Distinguishing different TM sources and sinks is essential for understanding changing dynamics across the NE Greenland shelf and other Arctic outflow regions which represent among the most climatically sensitive environments in the modern-day ocean (Mouginot et al., 2015). Despite their on-going retreat, there is limited knowledge to date of how the glacier cavities in North Greenland contribute to and potentially regulate TM (e.g., Cd, Co, Ni, Fe, Mn, and Cu) dynamics between dissolved and particulate phases. Furthermore, there is increasing evidence

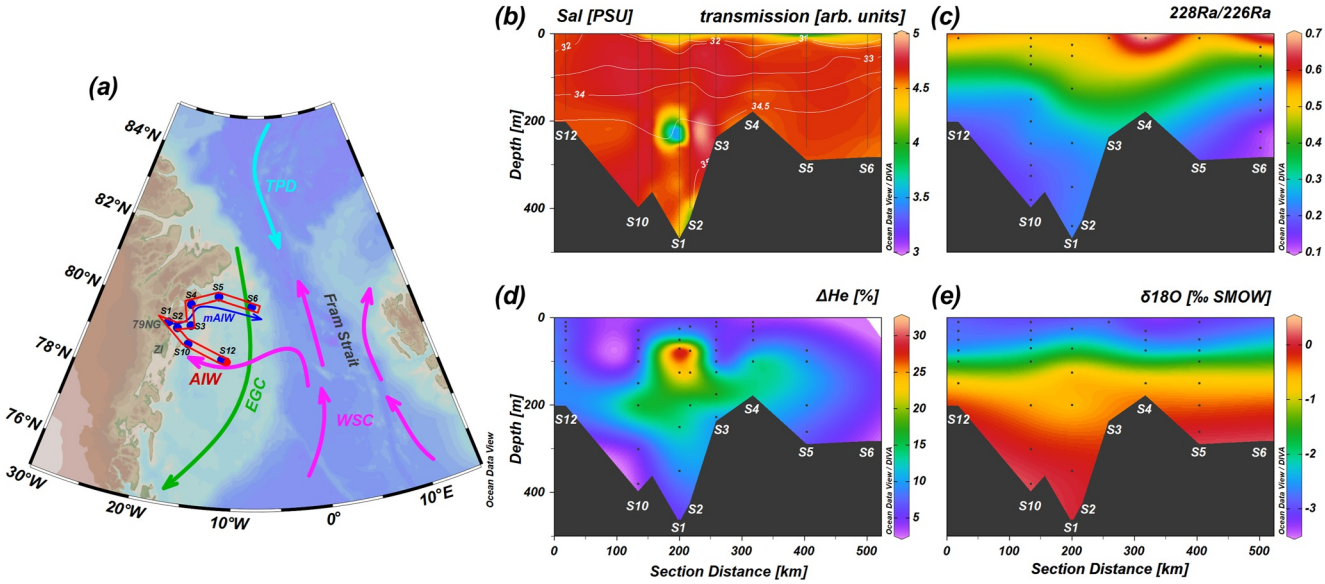

Figure 1. (a) Topography and studied stations on the Northeast Greenland shelf. Station names are as per Krisch, Hopwood, et al. (2021) for consistency with prior literature. The red ribbon defines the transect to show the distributions of physico-chemical parameters. Specifically, the transect follows the inflow of Atlantic Intermediate Water (AIW) (magenta arrow), a branch of the West Spitsbergen Current, from the station S12 in the East Greenland Current (EGC) to Norske Trough in the inner shelf (S10). Modified AIW exits from Nioghalvfjerdsbræ (79NG) front (S1) and 79NG bay (S2). Subsequently, mAIW flows to the Westwind Trough (WT) in the inner shelf (S3, inner WT), Dijmphna Sund (S4), Westwind Trough (S5, center WT), and further to the shelf break (S6). The southward transpolar drift exports Arctic surface waters into the EGC. Spatial distributions of (b) light transmission, (c) $^{228}Ra/^{226}Ra$, (d) He excess (ΔHe), and (e) $\delta^{18}O$ along the transect. The white lines illustrate salinity contours. The bathymetry of the section is adopted from the bottom depths of each station.

of strong lateral transfer of TMs across the Arctic in the TPD (Charette et al., 2020; Kipp et al., 2018), which may still be one of the most prominent drivers of TM dynamics in East Greenland (Krisch, Hopwood, et al., 2022). In order to investigate such processes using outflowing AIW properties, it is essential to discriminate local freshwater components from the Arctic outflow freshwater component, since both water masses manifest lower salinities and elevated dTM concentrations with respect to Atlantic waters (Achterberg et al., 2021; Charette et al., 2020; Gerringa et al., 2021).

Here, we present new labile particulate Cd, Ni, Cu, Al, Ti, V, and P and total particulate Cd, Co, Ni, Fe, Mn, Cu, Al, Ti, V, and P data from samples collected during the GEOTRACES cruise GN05 (PS100) in August 2016. Combined with published physical oceanographic data, macronutrients (NO_3 + NO_2, PO_4, and silicic acid), Ra isotopes (^{226}Ra, ^{228}Ra), He, $\delta^{18}O$, dTMs, and LpFe, LpCo, and LpMn data (Krisch, Hopwood, et al., 2021), we study the distributions of dTMs, LpTMs, and TpTMs on the NE Greenland shelf. We investigate the drivers of TM dynamics for the GEOTRACES "superstations" where all parameters were collected at high resolution in a highly coordinated fashion. These superstations cover a transect following the anticyclonic shelf circulation.

2. Geological Setting and Stations

The NE Greenland shelf (Figure 1a) is a dynamic region at the western boundary of the Fram Strait. The TPD, as a major outlet of Arctic surface waters, guides Eurasian shelf-derived materials toward the Fram Strait (Charette et al., 2020; Kipp et al., 2018). With a net southward flux of 1.1 ± 1.2 Sv, the Fram Strait is the only deep-water gateway for water exchange between the Arctic and North Atlantic Oceans (Fahrbach et al., 2001; Tsubouchi et al., 2018). Southbound transport of freshwater and associated nutrient signatures from the Arctic Ocean is a large source of trace elements to the Fram Strait (Krisch, Hopwood, et al., 2022; Torres-Valdés et al., 2013). Surface waters on the NE Greenland shelf, in a layer generally less than 100 m thick, are occupied by Polar Surface Water (PSW). A combination of PSW and Atlantic Water recirculating in the Fram Strait forms the southward EGC which then flows south along the Greenlandic coastline (de Steur et al., 2014; Richter et al., 2018; Rudels et al., 2005).

The NE Greenland shelf also receives discharge from the two large ZI and 79NG glaciers (Rignot & Mouginot, 2012). Saline AIW is directed through Norske Trough toward the NE Greenland coast (Figure 1a) where it induces basal melting of the 79NG terminus in the cavity underneath the floating ice tongue (Schaffer et al., 2020; Wilson & Straneo, 2015). Freshwater outflow from the ice tongue cavity largely reflects submarine melting by AIW, rather than seasonal subglacial discharge, and thus freshwater outflow occurs year-round with a mean flux of 0.63 ± 0.21 mSv estimated for 2016–2017 (Schaffer et al., 2020). The mixing between AIW and submarine meltwater from 79NG and ZI generates modified AIW (mAIW) which is 0.9°C cooler and fresher than the inflowing AIW (Mouginot et al., 2015; Schaffer et al., 2017, 2020; Wilson & Straneo, 2015). The mAIW flows clockwise on the NE Greenland shelf and is then incorporated into the EGC and likely flows southwards (Huhn, Rhein, Kanzow, et al., 2021; Laukert et al., 2017).

3. Sampling and Methods

3.1. Sampling

Samples were collected in August 2016 on the NE Greenland shelf (Figure 1a) during the PS100 GEOTRACES expedition (GN05) on RV Polarstern, corresponding to boreal late summer. TM, noble gas, and macronutrient sampling protocols and analyses are described in prior works (Huhn, Rhein, Kanzow, et al., 2021; Krisch, Hopwood, et al., 2021, 2022) and in Supporting Information S1, but for ease of access we provide a brief summary herein. Labile particulate Cd, Ni, Cu, Al, Ti, V, and P, and TpTM (Cd, Co, Ni, Fe, Mn, Cu, Al, Ti, V, and P) data reported herein are new determined in parallel with labile particulate Fe, Mn and Co described previously (Krisch, Hopwood, et al., 2021).

TM samples were collected using the ultra-clean CTD (ucCTD) rosette, equipped with 24 × 12 L GoFlo bottles following GEOTRACES sampling protocols (Cutter et al., 2017). The GoFlo bottles were subsampled in a clean room with 0.2 atm overpressure of filtered nitrogen gas. Samples for dTMs were filtered (Acropak 0.8/0.2 μm) into pre-cleaned LDPE (low density polyethylene) 125 mL bottles and acidified to pH 1.9 with HCl (UpA, ROMIL). Upon return to the laboratory, dTM sample aliquots were 10-fold pre-concentrated using an automated SeaFAST system (SC-4 DX SeaFAST pico; ESI) exactly as per Rapp et al. (2017). pTM samples were collected onto pre-acid leached Polyethersulfone Membrane filters (0.2 μm, Sartorius) with 1.2–4.1 L of seawater filtered per sample. Filters were stored at −20°C until analysis. Particles on filters were sequentially leached and digested as per Al-Hashem, Beck, et al. (2022) using a method adopted from Berger et al. (2008) and Cullen and Sherrell (1999). Briefly, samples were leached in a weak acid (25% Acetic Acid, Optima) and mild reducing agent (0.02 M hydroxylamine hydrochloride, 99.999% TM basis, Aldrich) for a total of 2 hr. Refractory particles were digested using a strong acid mixture of 50% nitric acid (Optima, Fisher Scientific) and 10% hydrofluoric acid (UpA grade, Fisher Scientific) (v/v %), with the sample filter adhered to the inner-wall of the digestion vessel and refluxed at 150°C for 15 hr. All TM concentrations (dTM, LpTM, and TpTM) were measured by high-resolution inductively coupled plasma-mass spectrometry (Thermo Fisher Element XR). For extensive details of quality control see Krisch, Hopwood, et al. (2021) and Supporting Information S1. Analyses of certified reference and consensus materials for newly reported LpTMs and TpTMs herein are shown in Table S1 in Supporting Information S1.

Samples for noble gases (He and Ne) and $\delta^{18}O$ were derived the large volume CTD (lvCTD) rosette. Helium and Ne samples were transferred from the water sampler into gas-tight copper tubes, and then analyzed by a fully automated ultra-high vacuum mass spectrometric system equipped with a two-stage cryogenic trap system by Huhn, Rhein, Kanzow, et al. (2021) following Sültenfuß et al. (2009). Stable oxygen isotopes ($\delta^{18}O$) were analyzed by a Finnigan MAT Delta-S mass spectrometer following Meyer et al. (2000). Radium isotope samples were obtained using in-situ pumps equipped with a 0.8 μm Supor (polyether sulfone) filter and passed through MnO_2-impregnated fiber to scavenge Ra isotopes from the filtrate (W. S. Moore, 2000). Then, natural Ra isotopic activities (^{226}Ra, ^{228}Ra) were measured by gamma spectrometry as per Rutgers van der Loeff et al. (2018).

3.2. Data Acquisition and Statistical Analyses

All data for lvCTD bottle samples and ucCTD observations were merged by their station labels and bottle depth (for details see Supporting Information S1) for locations where the two systems were deployed in succession (back-to-back events on the cruise, i.e., ∼2 hr apart). The almost identical physical oceanographic conditions (e.g.,

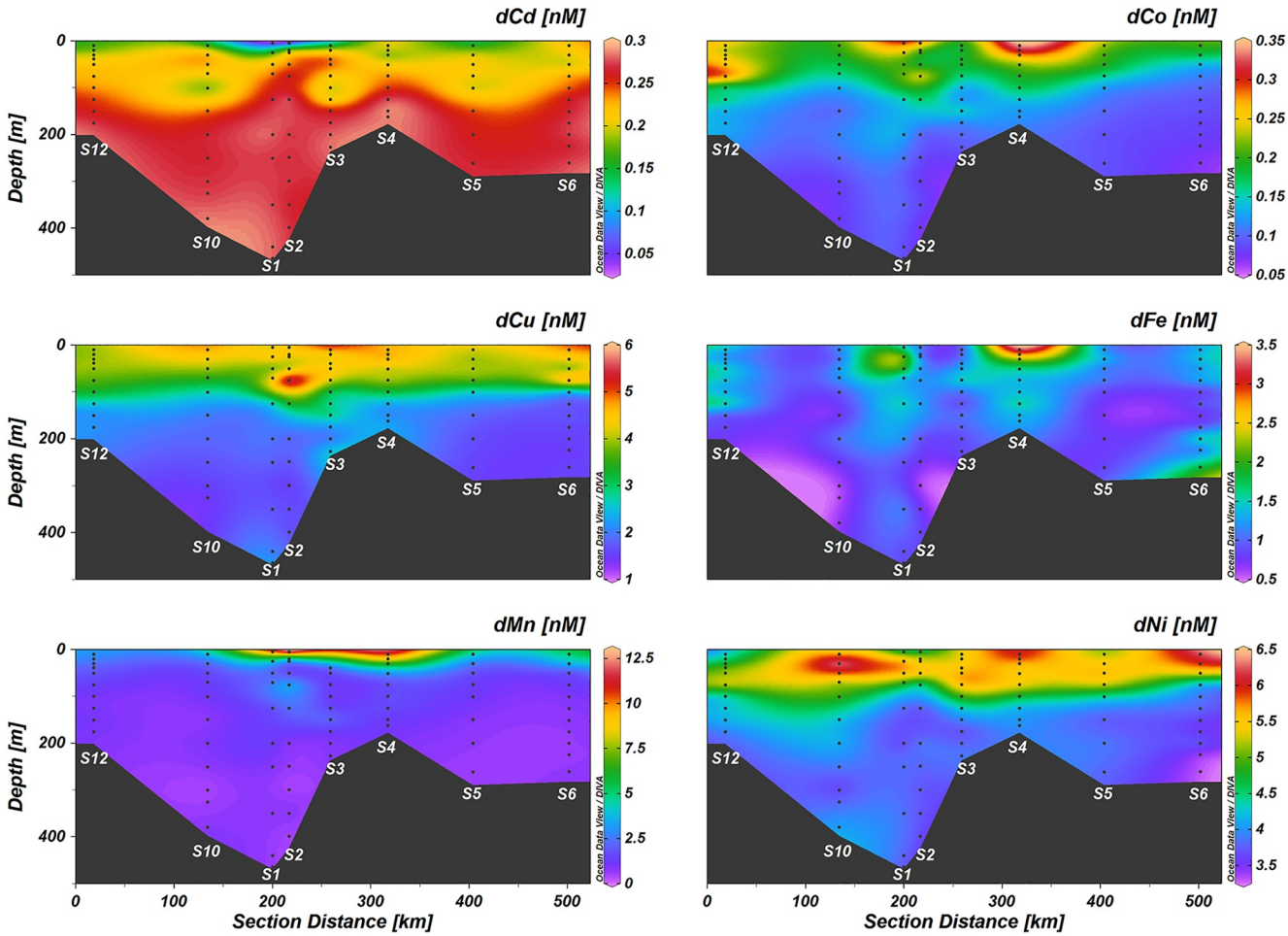

Figure 2. Sections of dissolved trace metals on the Northeast Greenland shelf along the section defined in Figure 1a.

salinity, potential temperature, and density) between lvCTD and ucCTD observations (Figure S1 in Supporting Information S1) demonstrate our data processing is reliable.

Principal component analysis (PCA) on the water column data were performed by *R* 4.2.0 with packages of *tidyverse* (Wickham et al., 2019) and *psych* (Revelle, 2017) using varimax rotations. Linear regressions between paired variables were calculated by *R* 4.2.0 with packages of *tidyverse* and *ggpmisc* (Aphalo, 2022). Figures 1–4 were made with Ocean Data View, version 5.6.2 (Schlitzer, 2021).

4. Results

All dTMs at the GN05 superstations demonstrated depth-dependent variations (Figure 2, Figure S2 in Supporting Information S1). Dissolved Co, Cu, Mn, and Ni showed significant surface (depth <10 m) enrichments and decreasing concentrations with increasing depth. Dissolved Co concentrations decreased from 0.20 to 0.30 nM in surface waters to generally below 0.10 nM at depths >100 m. Dissolved Ni concentrations increased from ~5 nM in surface waters to maxima of 5.5–6.5 nM at a depth of 50 m. Then, dNi levels dropped sharply to <4 nM at depths >100–150 m. Dissolved Cu profiles exhibited a pattern similar to dNi, with relatively high concentrations of 4–5 nM at depths <100 m and <2 nM at depths >100–150 m. Dissolved Mn concentrations declined sharply from surface maxima (>5 nM) to much lower concentrations (<1 nM) below the PSW. Dissolved Fe concentrations (0.56–3.35 nM, mean 1.21 nM) also generally showed surface enrichments, especially at the Dijmphna Sund station (station S4). Dissolved Cd illustrated different vertical profiles than other dTMs, with surface depletions (~0.05 nM at 79NG stations) and elevated concentrations at depth. At depths >100–150 m, the dCd concentration was maintained at 0.25–0.29 nM.

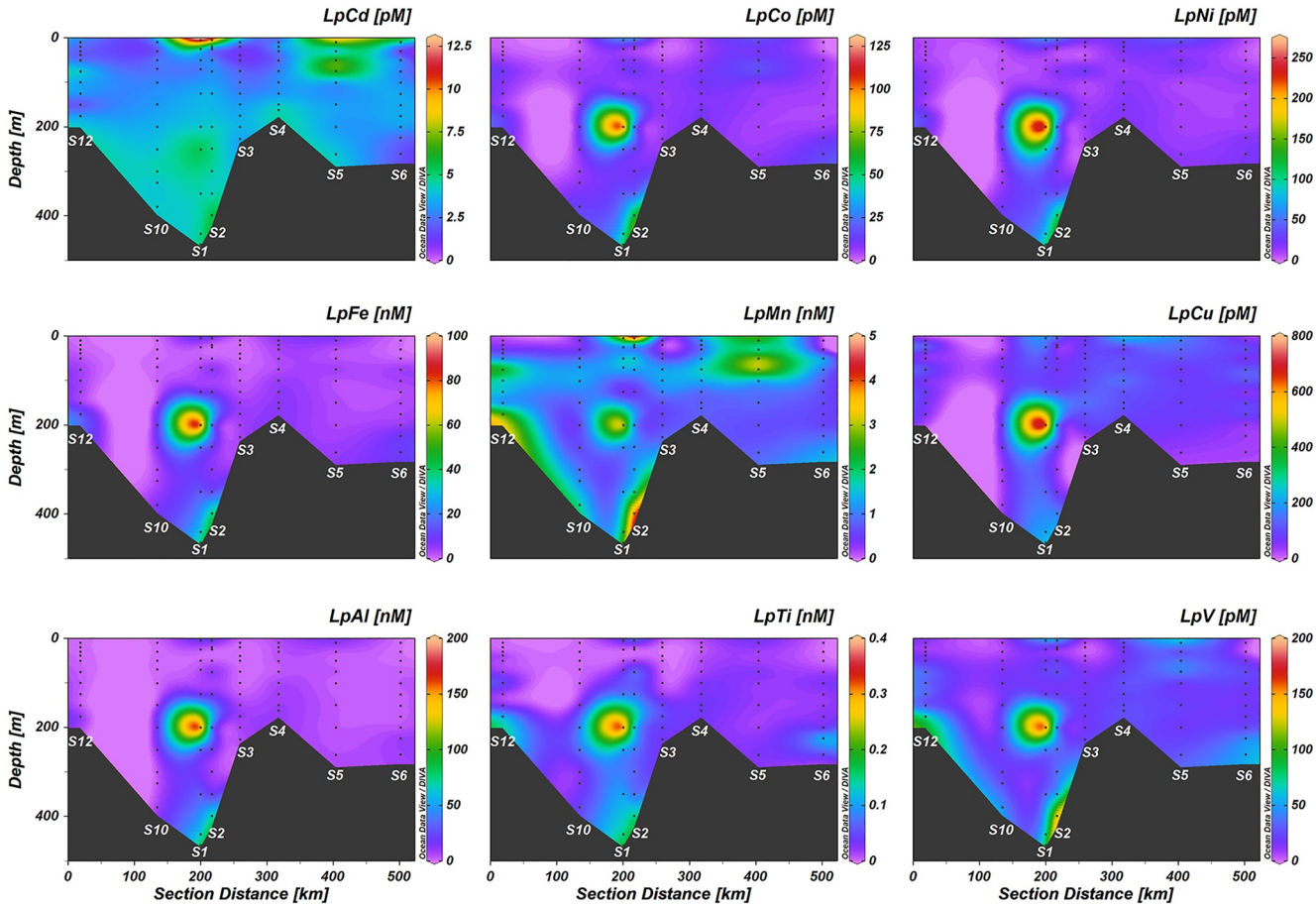

Figure 3. Sections of labile particulate trace metals on the Northeast Greenland shelf along the section defined in Figure 1a.

Except for the stations close to 79NG (stations S1 and S2), all other stations showed similar LpTM distribution profiles (Figure 3, Figure S3 in Supporting Information S1). Concentrations of LpAl, LpCo, LpCu, LpFe, and LpNi were more independent of depth than dTMs, showing averages of 4.27 ± 3.57 nM, 6.98 ± 4.11 pM, 83.5 ± 42.1 pM, 3.56 ± 2.86 nM, and 14.2 ± 6.9 pM, respectively. The LpCd concentrations decreased with depth from surface enrichment to about 2 pM at 50 m. Thereafter, LpCd concentrations generally increased with depth. Similarly, LpP showed strongly surface enrichments with concentrations of up to 38.8 nM in Norske Trough (station S10). Labile particulate P concentrations dropped to ∼2 nM at depths >50 m. In contrast, LpMn presented surface depletions with concentrations of <0.5 nM. The maximum LpMn concentrations (1.5–3 nM) occurred at depths of 50–75 m, just below the surface maxima of dMn. Then, LpMn levels dropped to <1 nM at 100–150 m and increased slightly with depth below. The concentrations of LpTi and LpV gradually increased with depth, from ∼5 pM (LpTi) and ∼10 pM (LpV) in near surface waters to ∼30 pM (LpTi) and 24–50 pM (LpV) at depths >300 m. In addition, both LpCd and LpMn exhibited a peak at depths of 50–100 m at the center Westwind Trough (WT) station (S5). All LpTMs showed some evidence of a peak at the deepest depth sampled (within ∼5 m of the sediment interface).

Water columns at the 79NG front (station S1) and in the 79NG bay (station S2) showed distinctive LpTM patterns. Both stations presented surface elevations of all LpTMs, especially for LpCd and LpMn, with respect to other stations. For instance, the surface LpCd content at 79NG front reached 12.6 pM, which was 2–4 times higher than at other stations. The surface LpMn concentrations increased from <0.5 nM at other stations to 4.5 nM in the 79NG bay. The 79NG front and 79NG bay stations exhibited bottom enrichments for all the investigated LpTMs. More strikingly, the 79NG front demonstrated extraordinarily high LpTM contents at a depth of 200 m. For example, the LpCo and LpNi contents reached 120 and 268 pM, respectively, one order of magnitude higher than at other stations.

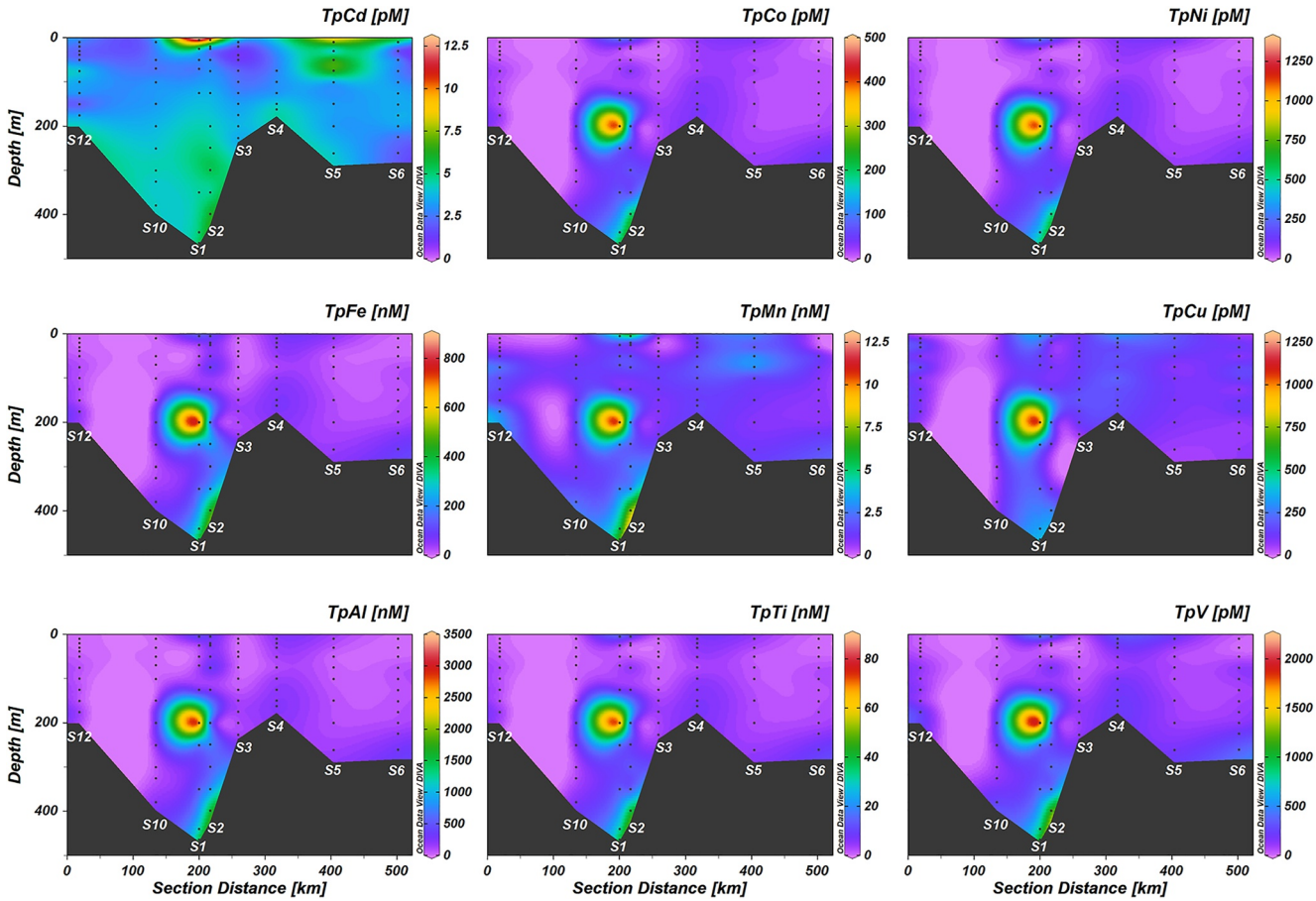

Figure 4. Sections of total particulate trace metals on the Northeast Greenland shelf along the section defined in Figure 1a.

The TpTM profiles on the NE Greenland shelf illustrated almost identical patterns to that of LpTMs (Figure 4, Figure S4 in Supporting Information S1). Except for the 79NG stations, TpAl, TpCo, TpCu, TpFe, and TpNi exhibited relatively independent variations with depth, showing average concentrations of 95.8 ± 74.5 nM, 16.7 ± 10.4 pM, 121.4 ± 54.3 pM, 29.1 ± 21.9 nM, and 46.6 ± 29.8 pM, respectively. Total particulate Cd and P presented surface enrichments with maximum concentrations of 8.12 pM and 62.5 nM, respectively. The concentrations of TpMn, TpTi, and TpV gradually increased with depth, showing average values of 1.24 ± 0.68 nM, 2.88 ± 2.13 nM, and 112 ± 79.4 pM, respectively. At the 79NG stations (station S1 and S2), all the investigated TpTMs and TpP showed dramatically elevated concentrations in surface waters, at a depth of 200 m, and in bottom waters. For instance, the TpAl and TpFe contents of the 79NG front station at 200 m increased to 3,367 nM and 891.8 nM, respectively, ~30 times higher than that at non-79NG stations. These concentrations are extremely high in a coastal oceanographic context - although similar to the limited values reported elsewhere in similar geographic contexts around Greenland (Kanna et al., 2020; Menzel Barraqueta et al., 2018).

5. Discussion

5.1. Statistical Analyses

The relationships between TMs and physico-chemical parameters were assessed using PCA (Figure S5 in Supporting Information S1). All parameters could be explained by a three-component model with cumulative variance of 80.7% and eigenvalues of 15.76 (rotated principal component 1, RC1), 12.70 (RC2), and 3.80 (RC3). The RC1 is comprised of significant positive loadings of all LpTMs and TpTMs and a negative loading of light transmission. A similar phenomenon was reported considering only Fe, Mn and Co distributions by Krisch, Hopwood, et al. (2021) with a maximum LpFe on the NE Greenland shelf coinciding with minimum light

transmission, suggesting a particle-rich layer exiting the glacier cavity. This component shows very low loadings with physical oceanographical parameters, indicating the distributions of LpTMs and TpTMs are negligibly controlled by water mixing. The RC2 exhibits strong positive loadings with all physical oceanographical parameters including depth, salinity, and density, reflecting the stratified water columns on the NE Greenland shelf and the conservative mixing of water masses (i.e., AIW, mAIW, and PSW). The RC2 has high positive loadings of $\delta^{18}O$ and negative loadings of ^{224}Ra and ^{228}Ra activities. Stable oxygen isotopes are an indicator for freshwater contributions since freshwater presents more negative $\delta^{18}O$ values than seawater (Azetsu-Scott & Tan, 1997; Bauch et al., 2011; Tiwari et al., 2018). Elevated ^{228}Ra is a typical feature of sedimentary input, which can reflect local sediment re-suspension and/or the intrusion of Arctic surface waters, as shelf-derived materials lead to elevated ^{228}Ra (half-life, $t_{1/2}$ = 5.75 years) concentrations, especially in the TPD (Kipp et al., 2018; Rutgers van der Loeff et al., 2018). All macronutrients showed significant positive loadings in RC2, indicating increasing concentrations with depth, which are typical for macronutrient profiles due to biological uptake in surface waters and remineralization of sinking phytoplankton cells at depth. Surface biological activity is further evidenced by the significant positive loading of dCd and negative loadings of fluorescence and pP in RC2 reflecting the parallel behavior of phosphate and dCd in marine systems (Boyle et al., 1976). Other dTMs, in contrast, mostly exhibit significant negative loadings in RC2, coinciding with surface enrichments of dMn, dCo, dNi, and dCu (Figure 2, Figure S2 in Supporting Information S1).

The RC3 is composed of strong positive loadings of ΔHe, ΔNe (the Δ stands for an excess above the equilibrium concentration), ^{226}Ra, and ^{228}Ra. This component possibly reflects the processes imprinting He-Ne systematics and Ra isotopes, for example, inputs of submarine meltwater and also sediments (Hohmann et al., 2002; Huhn, Rhein, Kanzow, et al., 2021; Loose & Jenkins, 2014; Rutgers van der Loeff et al., 2012). In addition, LpCd, TpCd, LpP, TpP, and LpMn showed moderate positive loadings in RC1 and moderate negative loadings in RC3. These results demonstrate that the association that Cd and Mn have with the lithogenic particle plumes is less prominent than that observed for other TMs close to the 79NG. Other processes are required to explain their distributions. These processes likely include biological coupling to PO_4 for Cd (Boyle et al., 1976) and photochemistry for Mn (Sunda & Huntsman, 1988; Sunda et al., 1983).

5.2. Dissolved TMs Distributions Are Mainly Controlled by Arctic Ocean Outflows

The significant positive correlations among depth, salinity, density, and $\delta^{18}O$ (Figure S5 in Supporting Information S1) indicate the mixing between water masses with contrasting salinities. Using simple linear regressions for dTMs and salinity (Figure S6 in Supporting Information S1), the dTM concentrations of the saline endmember, which should be AIW (Bourke et al., 1987; Schaffer et al., 2017), are calculated as (with 95% confidence levels): dCd, 0.28 ± 0.05 nM; dFe, 0.85 ± 0.14 nM; dMn, 0.14 ± 0.38 nM; dCo, 0.08 ± 0.01 nM; dNi, 3.65 ± 0.13 nM; and dCu, 1.71 ± 0.19 nM at an extrapolated salinity of 35. The dMn-salinity correlation is influenced by the extraordinary high dMn values in Dijmphna Sund (station S4); if these values are excluded, the endmember dMn of AIW would be 0.51 ± 0.21 nM. All these endmember AIW values are close to the dTM concentrations measured on the same cruise in the Fram Strait (Krisch, Hopwood, et al., 2022) (Table S2 in Supporting Information S1).

Except for dFe, with a relatively low correlation coefficient (R^2) of 0.36, all other dTMs display a strong correlation with salinity ($R^2 > 0.6$). The estimated zero salinity endmembers via linear regression are dCd <0 (−0.54 ± 0.12 nM), dMn 25.8 ± 3.7 nM (also excluding the extraordinarily high dMn values in Dijmphna Sund), dCo 1.54 ± 0.16 nM, dNi 22.6 ± 2.0 nM, dCu 29.2 ± 2.7 nM. Although we cannot discriminate different freshwater sources using salinity alone, meltwater from the NE Greenland glaciers (e.g., 79NG and ZI) is clearly not a dominant source of freshwater based on the volume flux estimates (e.g., ∼0.6 mSv; Schaffer et al., 2020). Instead, freshwater signals on the shelf are mainly supplied by Arctic Ocean outflow (de Steur et al., 2018). Elevated concentrations of dTMs in surface waters are a typical feature of the Arctic Ocean (Charette et al., 2020; Gerringa et al., 2021) (e.g., zero-salinity endmember dNi and dCu of Arctic surface waters are 30.6 and 30.1 nM, respectively. Table S2 in Supporting Information S1).

Furthermore, surface enrichments of dTMs coincided with increased $^{228}Ra/^{226}Ra$ ratios on the NE Greenland shelf (Figure 5). Radium-228 ($t_{1/2}$ = 5.75 years) and ^{226}Ra ($t_{1/2}$ = 1,600 years) are both non-particle reactive and continuously released from the decay of sediment-bound thorium (Th) isotopes. Due to the disproportionately high fluxes of shelf-derived materials into the Arctic Ocean (Aagaard & Carmack, 1989), Arctic surface

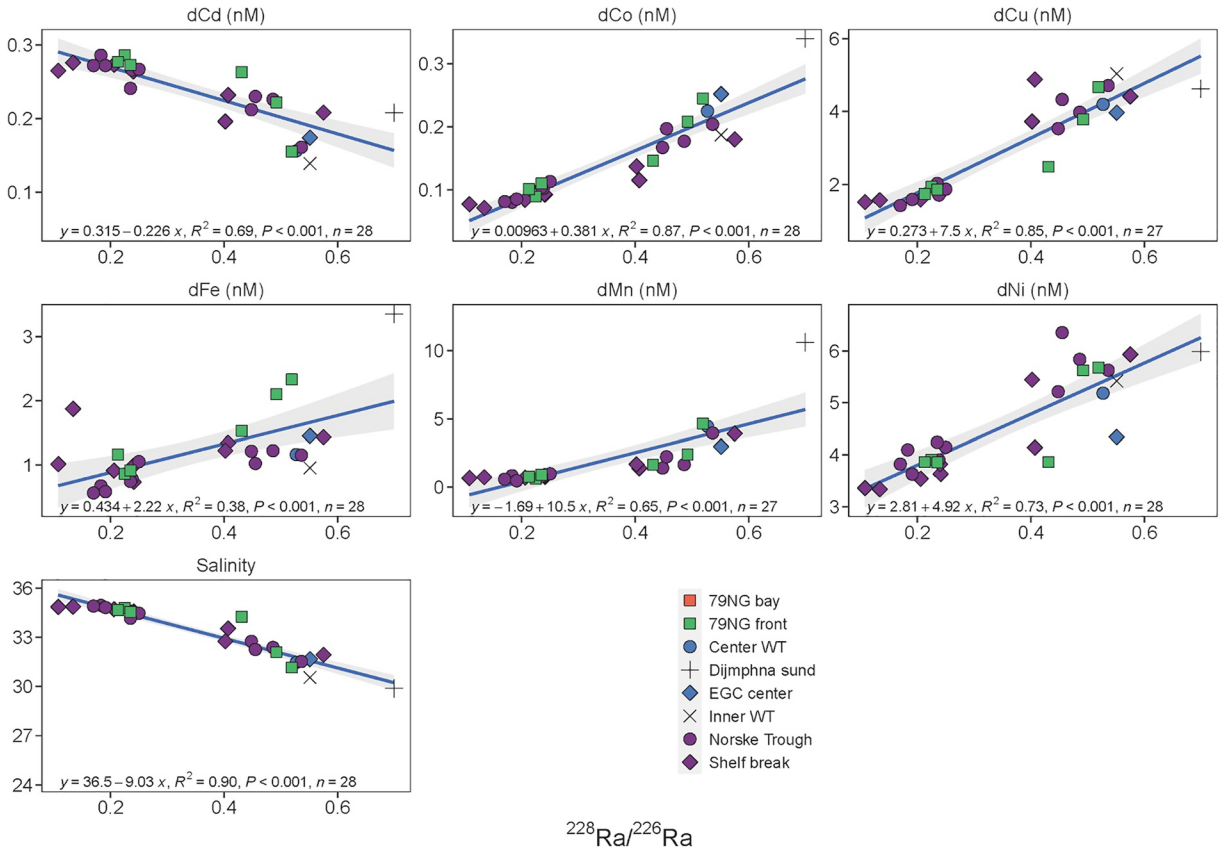

Figure 5. Correlations between dissolved trace metals (dCd, dCo, dCu, dFe, dMn, and dNi), salinity and $^{228}Ra/^{226}Ra$ ratios of water columns on the Northeast Greenland shelf. Note that radium isotopes were not available for the near surface samples from 79NG front and 79NG bay. The linear regression models (blue lines with 95% confidence levels) are therefore not affected by the surface glacial runoff of the 79NG. *n* indicates the number of samples in the linear regression models.

waters (and TPD) are characterized by strongly enriched ^{228}Ra concentrations and elevated $^{228}Ra/^{226}Ra$ ratios (Kipp et al., 2018; Rutgers van der Loeff et al., 2018). Although local submarine meltwater and shelf-derived sediment will also produce elevated $^{228}Ra/^{226}Ra$ ratios, such local processes will not create strongly decreased salinity since the contribution of submarine meltwater is less than 2% on the NE Greenland shelf (Huhn, Rhein, Kanzow, et al., 2021). The significant negative correlation between $^{228}Ra/^{226}Ra$ and salinity (Figure 5) and the surface enrichment of ^{228}Ra close to the shelf break (Figure 1) should therefore mostly reflect the intrusion of Arctic surface waters. The significant positive correlations between dTMs (dCo, dCu, dFe, dMn, and dNi) and $^{228}Ra/^{226}Ra$ (Figure 5), therefore, suggest that these dTMs on the NE Greenland shelf should be mostly controlled by southward flowing Arctic surface waters carried by the TPD rather than local signals from Greenlandic glaciers (Ardiningsih et al., 2020; Krisch, Hopwood, et al., 2022).

5.3. The 79NG Cavity Contribution to dTM Supply Derived From Helium Excess

The physico-chemical characteristics of outflowing mAIW are still distinguishable on the NE Greenland shelf despite the relatively small volume of 79NG subglacial freshwater discharge to the shelf (0.63 ± 0.21 mSv) compared to the Arctic outflow (1.1 ± 1.2 Sv) (Krisch, Hopwood, et al., 2021, 2022; Schaffer et al., 2020; von Albedyll et al., 2021). Due to the long residence time (~162 days, data from GN05 cruise) of inflowing AIW inside the subglacial cavity (Schaffer et al., 2020), the freshwater signals in the mAIW (denoted as submarine meltwater) may reflect extensive homogenization and equilibration of AIW with particle and dissolved inputs from ice melt, and sediment-water exchange. Cavity outflow has previously been observed for dFe and dissolved lead (dPb) at 79NG (Krisch, Hopwood, et al., 2021; Krisch, Huhn, et al., 2022). Here, we used noble gases as a tracer to distinguish the influence of submarine meltwater from Arctic waters on TM distributions on the NE Greenland shelf, following the methods of Huhn, Rhein, Kanzow, et al. (2021). The main source of oceanic He is

gas exchange with the atmosphere (Hohmann et al., 2002; Loose & Jenkins, 2014). Helium is trapped in the ice matrix during the formation of glacier ice. Such excess He (ΔHe) is completely dissolved in the meltwater during submarine melting at depth, while no notable ΔHe will be observed for surface runoff and intruded Arctic surface waters because of equilibration with the atmosphere (Kim et al., 2016; Loose & Jenkins, 2014). The warm and saline AIW in Norske Trough station is characterized by the highest salinity and $\delta^{18}O$ across the NE Greenland shelf, and a ΔHe of about 3.6% which is slightly lower than the natural oversaturation of He in ocean waters (Loose & Jenkins, 2014). Most samples on the NE Greenland shelf are characterized by a sharp decrease in $\delta^{18}O$ and salinity, with ΔHe of up to 5% (Figure S7 in Supporting Information S1). This pattern is explained by the mixing between AIW and Arctic surface waters, since ΔHe of 5% is very similar to the background ΔHe from both the Fram Strait and south Greenland (e.g., Huhn, Rhein, Kanzow, et al., 2021; Rhein et al., 2018).

The incorporation of submarine meltwater results in marked increases in ΔHe with slight reductions in $\delta^{18}O$ and salinity (Figure S7 in Supporting Information S1). The samples following this pattern mostly occur at the 79NG front (station S1) and 79NG bay (station S2) with depths of 70–250 m, coinciding with the exiting of mAIW from the 79NG cavity at 90–250 m (Schaffer et al., 2020). Therefore, the meltwater signals on the NE Greenland shelf are predominantly sourced from the 79NG cavity (Huhn, Rhein, Kanzow, et al., 2021). By excluding the two samples (with a depth of 75 m) significantly affected by Arctic surface flows, the endmember ΔHe of the submarine meltwater is estimated as 1,120‰ ± 121‰ (95% confidence level) using a meltwater endmember salinity of 0. This estimation is comparable to reported pure meltwater values (e.g., 1,280‰; Beaird et al., 2015; Loose & Jenkins, 2014). The mAIW samples show significant positive correlations between dTM (dCo, dCu, dFe, and dMn) concentrations and ΔHe (Figure S8 in Supporting Information S1), indicating that the source of these dTMs in mAIW is submarine meltwater, despite the overall dTM distributions on the NE Greenland shelf being mainly controlled by the mixing between Arctic Ocean outflows and AIW. Using the endmember ΔHe of 1,280% for meltwater (Huhn, Rhein, Kanzow, et al., 2021), the apparent endmember dTM concentrations of the submarine meltwater are estimated as 5.15 ± 2.49 nM dCo, 75.9 ± 102 nM dCu, 31.4 ± 41.2 nM dFe, and 107 ± 63.7 nM dMn (with 95% confidence levels). As per extrapolations using salinity, these regressions produce apparent concentrations inclusive of non-conservative processes affecting the concentration of dTMs during the timeframe since the release of submarine meltwater. These concentrations are 1–3 orders of magnitude higher than that in the Fram Strait (Krisch, Hopwood, et al., 2022) and EGC in Southeast Greenland (Achterberg et al., 2021), but similar to endmember values derived from summer coastal/fjord data around south/west Greenland (Krause et al., 2021; van Genuchten et al., 2022), demonstrating the 79NG submarine meltwater is a strong local source of these dTMs. For instance, the dCo content of the meltwater is more than 60 times higher than that of AIW. Hence, 2% addition of meltwater would theoretically double the dCo concentration of mAIW exported from the 79NG cavity.

Estimations of the apparent endmember dTM concentrations in submarine meltwater could be biased to higher concentrations because a fraction of dTMs is likely provided by cavity sediment-seawater exchange rather than the ice melt. This is reflected by the significant positive correlations between dTMs (especially Co, Cu, Fe, and Mn) and Δ(He/Ne) values (Figure S9 in Supporting Information S1) because elevated He/Ne ratios suggest additional ^{4}He from α-decay of bedrock in the glacier cavity, and hence potentially indicate sediment signals. Furthermore, the 79NG front samples illustrated elevated dTM concentrations, ΔHe, and $^{228}Ra/^{226}Ra$ ratios. Despite the limited available samples, the similar variation patterns of these parameters suggest that dTMs in the mAIW may be affected by sediment re-suspension. Nevertheless, based on concentrations alone, there is no conclusive method to distinguish elevated dTMs in mAIW released from cavity sediments or contributed by both sediments and submarine melting. Yet, it was noted that the close to crustal $\delta^{56}Fe$ signal of dFe in mAIW (+0.07‰ ± 0.09‰) supports a primarily sedimentary origin for dFe as this is clearly delineated from the isotopically light signal normally associated with glacial runoff (Krisch, Hopwood, et al., 2021; Stevenson et al., 2017).

The apparent endmember dNi and dCd concentrations of the meltwater are calculated as 6.12 ± 21.9 and 0.026 ± 1.52 nM, respectively; but both estimates have high uncertainties. The distribution of total N and phosphate in mAIW is unlikely affected by subglacial meltwater addition as both $NO_3 + NO_2$ and PO_4 show poor correlations with ΔHe (Figure S10 in Supporting Information S1). Of the three macronutrients, only silicic acid shows relatively high correlation with ΔHe ($R^2 = 0.53$) with an intercept of 28.7 ± 27.9 μM, demonstrating that subglacial meltwater is potentially a source of silicic acid to the NE Greenland Shelf. The p value of >0.05 of the silicic acid—ΔHe correlation in mAIW suggests, however, that other factors besides subglacial meltwater addition affect silicic acid discharge to the shelf, with vertical remineralization clearly dominant (as shown by the PCA, Figure S5 in Support-

ing Information S1). On a Greenlandic scale, only few measurements of dissolved silicic acid have been conducted in subglacial discharge, but our values are similar to those inferred from a fjord silicic acid budget in West Greenland (Meire et al., 2016) and in agreement with computed or measured endmember values in fjord systems of East Greenland (5.8 ± 1.8 to 40.2 ± 4.1 μM as per Cape et al. (2019) and Paulsen et al. (2017)).

5.4. Controlling Factors of LpTMs and TpTMs

The similarity in LpTM and TpTM profiles across the NE Greenland Shelf indicates that their distributions is largely determined by the same sources and/or regulated by similar processes. There are, however, important differences in pTM concentrations between 79NG stations and non-79NG stations. At non-79NG stations, all TMs except Cu, show generally decreasing LpTM and TpTM concentrations across the salinity gradient (Figures S11 and S12 in Supporting Information S1). Despite the relatively low correlation coefficients, which may be caused by the elevated pTM concentrations from turbulence in Dijmphna Sund, the similar variation patterns of LpTMs and TpTMs with salinity suggest that pTMs on the NE Greenland shelf are mainly controlled by the mixing between Arctic surface waters and AIW. The relatively lower pTM concentrations in the low-salinity endmember of non-79NG stations indicates the intruded Arctic surface waters are depleted in LpTMs and TpTMs. This is probably attributed to a removal of pTMs by sedimentation, particle aging, and/or solubilization during lateral transportation of Arctic Ocean outflows (Charette et al., 2020). In contrast, AIW is generally characterized by high pTM concentrations and could act as a major source of LpTMs and TpTMs (e.g., Achterberg et al., 2021) to the NE Greenland shelf.

On the other hand, LpTM and TpTM levels were strongly elevated in the middle and bottom layers of the water columns at the 79NG front (station S1) and 79NG bay (station S2) stations (Figures 3 and 4), suggesting that the 79NG cavity outflow was a strong source of pTMs. However, using ΔHe as a tracer, the LpTMs (Figure 6) and TpTMs (Figure S13 in Supporting Information S1) in mAIW manifest decreasing trends with increasing ΔHe levels. This suggests that pTMs maxima in the 79NG cavity outflow are likely not directly sourced from submarine melting. Instead, the elevated LpTM and TpTM levels in mAIW are mainly attributed to the re-suspension of sediment particles. This statement is supported by the decoupling of pTM and ΔHe plume in the cavity outflow. Whist the maximum ΔHe occurs at ∼70 to 100 m at 79NG stations (Figure 1), the maximum pTM concentrations were observed at a depth of ∼200 m (Figures 3 and 4), reflecting sinking and re-suspension of cavity-derived sediment particles. These particles may be derived from bottom sediments and bedrocks in the cavity, or sediments entrained in the glacier, or a combination of both. However, we cannot distinguish the sediment sources since all these sediment signals may have been homogenized in the cavity.

Total particulate Al, Ti, and V on the NE Greenland shelf are significantly correlated and their ratios are almost identical to that of upper continental crust (Rudnick & Gao, 2003) (Figure S14 in Supporting Information S1), suggesting Al, Ti, and V discharge to the shelf to be lithogenic in origin. The significant positive correlations between most LpTMs (except for LpCd) and TpAl, TpTi, and TpV indicate that these LpTMs in the water columns on the NE Greenland shelf are mostly hosted in lithogenic particles with limited or negligible biogeochemical processing (Figure 7). In contrast, LpCd may have been affected by biogenic particles as suggested by its relatively higher correlation coefficient (R^2 of 0.36) with TpP compared to other LpTMs. Combined with the coincidence between turbid layers and increased pTM levels (Figures 3 and 4), these results suggest that particles and the associated metals in mAIW exiting the 79NG cavity are probably sourced from the disturbance of lithogenic sediment particles by the overturning cavity flow (Krisch, Hopwood, et al., 2021; Wilson & Straneo, 2015).

5.5. Dynamics Between dTMs and pTMs

The overall distributions of dTMs and LpTMs were generally coupled in the water column across the NE Greenland shelf. Only samples at the 79NG stations (station S1 and S2) (with low light transmission and salinity) evidenced some degree of decoupling of dTM concentrations from (labile) particulate inputs. All other samples on the shelf illustrate almost constant dissolved fractions of labile species (defined as dTM/(dTM + LpTM)). For dCd, dCu, and dNi, dTM/(dTM + LpTM) ratios were close to 1, demonstrating that these labile TMs are mainly hosted in dissolved phases (Figure 8, Figure S15 in Supporting Information S1). In the case of Mn and Fe, dissolved and labile particulate phases are equally important, with dMn/(dMn + LpMn) and dFe/(dFe + LpFe) ratios mostly (first–third quartiles) in the ranges of 0.46–0.74 and 0.15–0.41, respectively. The variations of

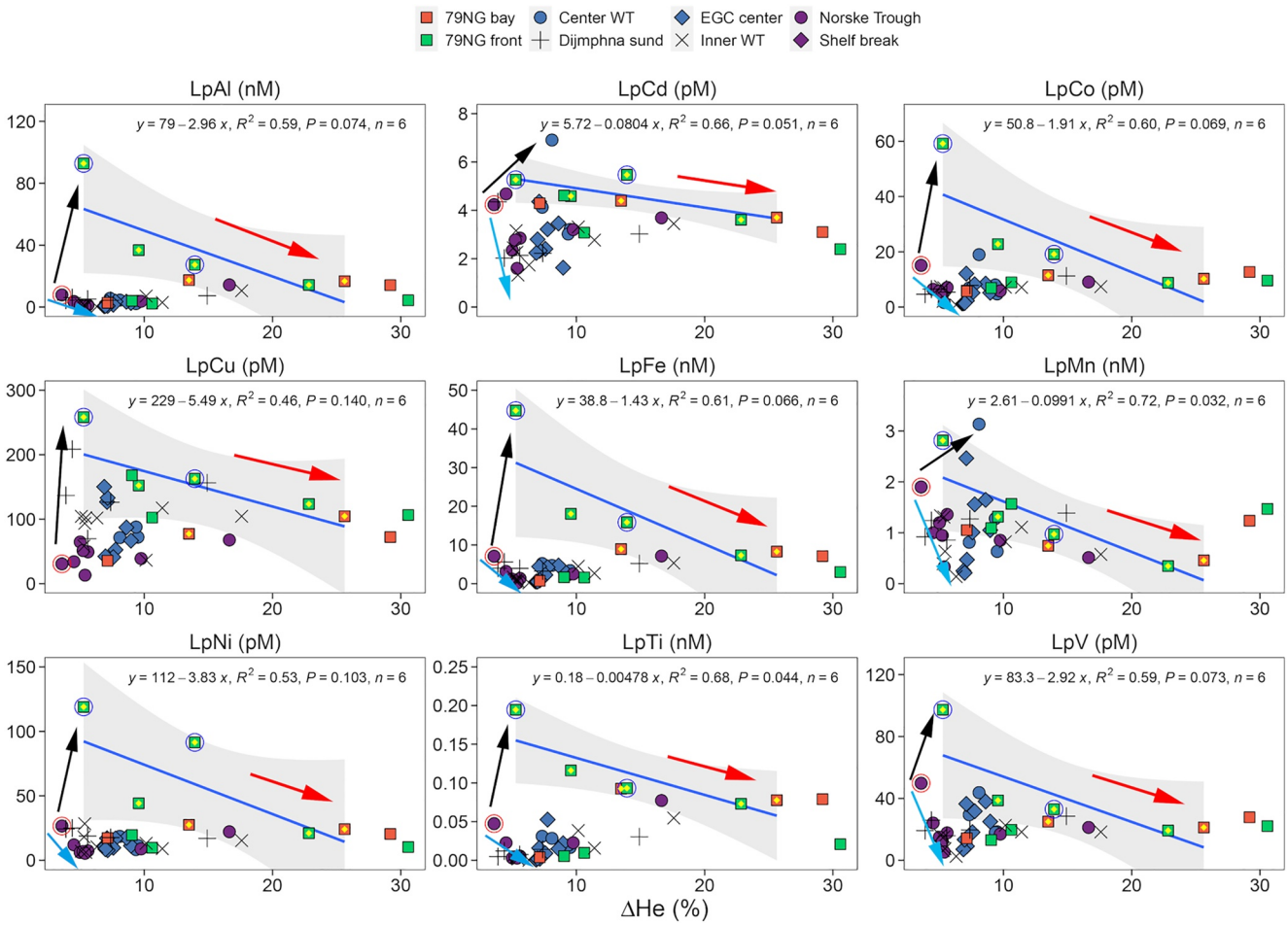

Figure 6. Changes of labile particulate trace metals with helium excess (ΔHe) on the Northeast Greenland shelf. Blue arrows indicate the involvement of Arctic surface waters, while red arrows suggest the addition of meltwater. Black arrows demonstrate the influence of sediment particles. The red encircled sample represents the inflowing Atlantic Intermediate Water (AIW), while the blue encircled samples indicate high turbidity (defined as light transmission <4.4). Linear regression models (blue lines with 95% confidence levels) only apply to the 79NG samples with depths >100 m (highlighted with yellow diamonds) to demonstrate the influence of modified AIW exiting the 79NG cavity. *n* indicates the number of samples in the linear regression models.

dTM/(dTM + LpTM) ratios across the salinity gradient suggest the dTM-LpTM dynamics largely reflect mixing between two different source waters: Atlantic-derived AIW and Arctic Ocean Outflows. Specifically, dCd/(dCd + LpCd) decreases slightly with decreasing salinity, indicating the depletion of dCd in Arctic surface waters with respect to AIW, attributed to an efficient biological drawdown of dCd (R. Zhang et al., 2019). Cobalt, Fe, and Mn demonstrate significantly increased dTM/(dTM + LpTM) ratios with decreasing salinity. The high correlations observed for dTM/(dTM + LpTM) and salinity on the NE Greenland shelf suggest the relatively conservative mixing between dTM-rich Arctic surface waters (which has experienced long-range transportation) and LpTM-rich AIW. The elevated dTM/(dTM + LpTM) ratios in the Arctic surface waters relative to AIW could be ascribed to the scavenging removal of LpTMs during lateral transportation, since Co, Mn, and Fe are all scavenged-type metals (Charette et al., 2020; Honeyman et al., 1988; Lohan & Tagliabue, 2018) alongside the efficient cross-Arctic transport of dTMs stabilized by organic materials (Bundy et al., 2020; Slagter et al., 2017).

The significantly elevated LpTM levels in the mAIW exiting the 79NG cavity produced relatively low dTM/(dTM + LpTM) ratios compared to other stations (Figure 8, Figure S15 in Supporting Information S1). LpTM enrichments in these samples were closely related to decreased light transmission (i.e., increased turbidity). The turbid layer at 200 m is associated with the outflow of mAIW, while the bottom turbid layer is likely due to the re-suspension of sediment particles (Figure 1b). However, large enrichments of dTMs and significant ΔHe are absent in these turbid layers (Figure 1d), indicating that the LpTM maxima in the turbid layers are decoupled from the submarine meltwater. This is consistent with previous interpretations of the Ra and Fe isotopic signatures

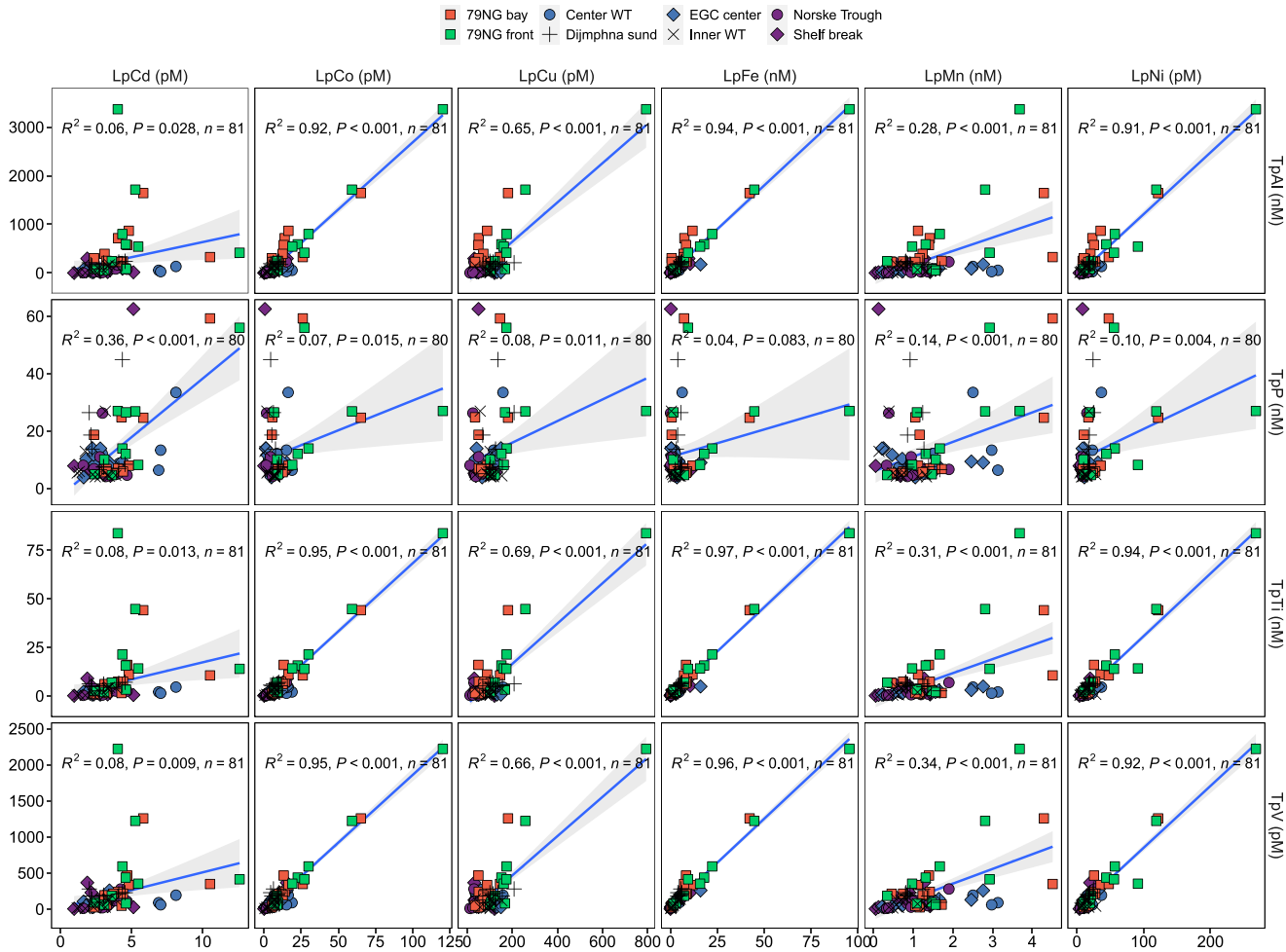

Figure 7. Correlation matrix between labile particulate trace metals (LpCd, LpCo, LpCu, LpFe, LpMn, and LpNi) and total particulate trace elements (TpAl, TpTi, TpV, and TpP) in the water column on the Northeast Greenland shelf. Linear regression models (blue lines with 95% confidence levels) are applied to all samples. *n* indicates the number of samples in the linear regression models.

from station S1 within the 200 m turbidity layer (Krisch, Hopwood, et al., 2021). All TMs illustrate declined dTM/(dTM + LpTM) ratios in the turbid layer relative to the inflowing AIW, indicating a major source of LpTMs from re-suspension of sediment particles carried by the cavity outflow.

A similar phenomenon is observed for variations in labile particulate fractions of TMs (LpTM/TpTM) on the NE Greenland shelf. Except for Cd with a LpCd/TpCd ratio close to 100%, the labile particulate fractions of all the other TMs manifest two mixing paths with Arctic waters and submarine meltwater, respectively (Figure S16 in Supporting Information S1, Figure 8). AIW is characterized by relatively low labile particulate fractions, for example, ~0.5 for Cu, ~0.4 for Co, ~0.1 for Fe, ~0.03 for Al, and <0.01 for Ti. Therefore, the mixing between Arctic surface waters (relatively high LpTM/TpTM ratios, ΔHe = ~5‰) and AIW (low LpTM/TpTM ratios, ΔHe = 3.6‰) will result in elevated labile particulate fractions and relatively constant ΔHe values with increasing contribution of Arctic surface waters. As a result, the labile particulate fractions of Cu, Co, Mn, and Ni all show maxima (LpTM/TpTM close to 1) near the surface at depths of 25–75 m on the NE Greenland shelf. The relatively higher LpTM/TpTM ratios (especially for bio-essential TMs, e.g., Cd, Co, Cu, Mn, and Ni) in Arctic surface waters relative to AIW suggest that TMs hosted in lithogenic sedimentary particles have been efficiently removed during lateral transportation across the Central Arctic or biogeochemically processed to form more labile fractions. Additionally, the oxidative precipitation and scavenging of dTMs like Fe and Mn will also result in increased LpTM/TpTM ratios. Furthermore, ongoing dynamic exchange between dTMs and biogenic particles in the Arctic outflow is supported by the elevated LpP and TpP concentrations with decreasing salinity in the water column on the NE Greenland shelf (Figure S17 in Supporting Information S1).

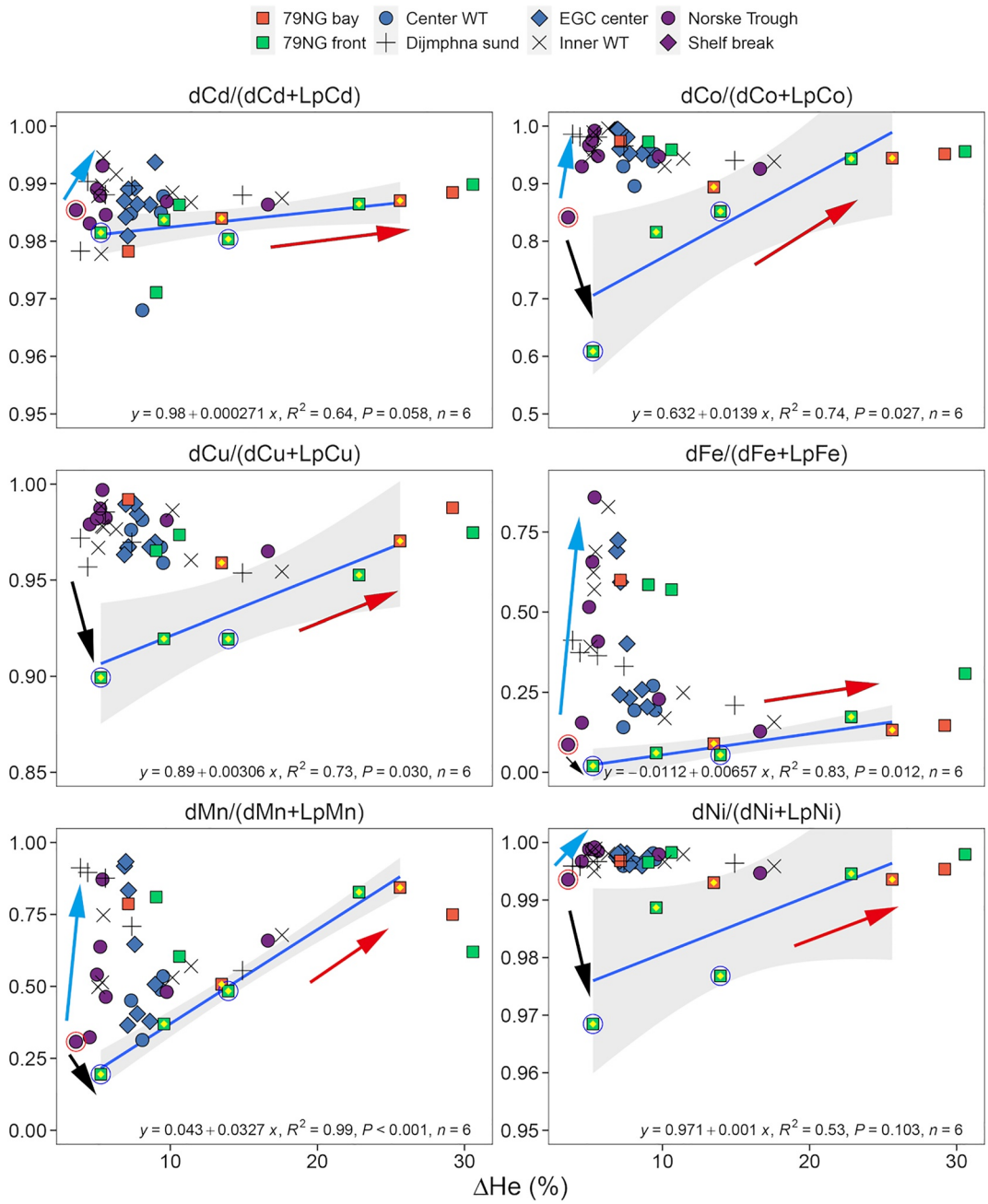

Figure 8. Variations of dTM/(dTM + LpTM) ratios with helium excess (ΔHe) on Northeast Greenland shelf. Blue arrows indicate the involvement of Arctic surface waters, while red arrows suggest the addition of meltwater. Black arrows demonstrate the potential influence of sediment particles. The red encircled sample represents the inflowing Atlantic Intermediate Water, while the blue encircled samples indicate high turbidity. Linear regression models (blue lines with 95% confidence levels) only apply to the 79NG samples with depths >100 m (highlighted with yellow diamonds). *n* indicates the number of samples in the linear regression models.

5.6. The 79NG Influence on dTMs and pTMs Beyond the Glacial Cavity

The cavity flow with overturning fluxes of 46 ± 11 mSv (Schaffer et al., 2020) transports abundant dTMs from the 79NG cavity onto the NE Greenland shelf (Krisch, Hopwood, et al., 2021, 2022). Despite the extensive dilution of meltwater during lateral transport (Huhn, Rhein, Kanzow, et al., 2021), up to 1% meltwater occurs downstream of 79NG, for example, Dijmphna Sund (station S4, depth 100 m) and Inner WT (station S3, depths >100 m) have

0.5%–1.2% meltwater contributions, and center WT (station S5) and EGC center (station S12) exhibit meltwater proportions of 0.2%–0.5%. As a result, dTMs in the water columns of Dijmphna Sund, Inner WT, center WT, and EGC center, with depths generally >100m, are largely constrained by the mixing between AIW and submarine meltwater (Figure S8 in Supporting Information S1). Based on the estimated meltwater contributions (Figure S7 in Supporting Information S1) and the apparent endmember dTM concentrations of the submarine meltwater, about 10%–25% dCo in center WT and 5%–20% dCo in EGC center on the outer NE Greenland Shelf were supplied by the submarine meltwater from the 79NG cavity. Up to 60% dMn in Dijmphna Sund and Inner WT was sourced from the 79NG cavity ascribed to the high apparent dMn concentrations in the meltwater endmember (which is similar to observations in other glaciated Arctic regions) (Kandel & Aguilar-Islas, 2021; van Genuchten et al., 2022).

Re-suspended particles brought by the overturning cavity flow exiting the 79NG cavity form potentially an important source of pTMs to the NE Greenland shelf with the majority of glacier-derived particulates, however, likely being list near the glaciers grounding line (Mayer et al., 2018; Schaffer et al., 2020). The mixing between particle-rich AIW and particle-depleted Arctic surface waters illustrates a decrease in LpTMs with decreasing salinity and almost constant ΔHe (Figure S11 in Supporting Information S1, Figure 6). However, this phenomenon is absent in the dynamics of LpCu, as almost all samples present higher LpCu contents than the inflowing AIW. In addition, elevated LpCo, LpMn, and LpCu concentrations relative to AIW occur in Dijmphna Sund (station S4), inner WT (S3), center WT (S5), and EGC center (S12) stations. Especially in the near-surface samples (<100 m depth) of Dijmphna Sund and center WT, the LpTM and TpTM levels were systematically higher than other stations across the salinity gradient (Figures S11 and S12 in Supporting Information S1). Elevated LpCu and LpMn levels in Dijmphna Sund are likely the consequence of enhanced sediment turbulence over the sill (Arndt et al., 2015; Schaffer et al., 2020). Further offshore, elevated LpTM concentrations in the center WT (station S5) are likely related to the higher productivity observed at this site (Lara et al., 1994; Pesant et al., 1998). Furthermore, the dMn and dCo concentrations in the Dijmphna Sund near surface waters far exceed those both in Arctic surface waters and AIW and indicate a local source (Figure S8 in Supporting Information S1). The dFe levels were also elevated with respect to the expected TPD contribution. These results indicate that dTM concentrations were further increased locally perhaps due to solubilization of TMs from sediment particles.

5.7. Surface Runoff

In addition to submarine meltwater, the surface runoff from 79NG is potentially a source of TMs. Two near surface (depth ∼5 m) samples from the 79NG stations showed systematically different characteristics than other samples, for example, lower salinities and higher dMn concentrations (Figure S6 in Supporting Information S1). Because such a phenomenon was absent at non-79NG stations, it was not likely a result of sea-ice melt (e.g., Tovar-Sánchez et al., 2010), although the cruise was conducted during the peak of the melting season (August 2016). Therefore, the surface waters in the 79NG stations could have been influenced by surface glacial runoff. Unfortunately, we cannot calculate the endmember dTM concentrations of the surface runoff due to the paucity of available data of tracers such as ΔHe and Ra isotopes and limited number ($n = 2$) of samples.

The postulated surface runoff significantly elevated the LpTM and TpTM levels at 79NG stations (Figures 3 and 4). For instance, LpCd, LpNi, and LpCu concentrations were double in surface waters near 79NG relative to other surface samples. The average LpCo in the surface waters near 79NG (26.8 pM) was more than five times higher than the average levels (4.85 pM) on the NE Greenland shelf. All TMs, especially Fe, Co, Ni, Cu, and Mn, showed lower dTM/(dTM + LpTM) ratios than the non-79NG samples (Figure 8, Figure S15 in Supporting Information S1), suggesting surface runoff contributed elevated LpTMs to surface waters, probably reflecting the source of sediments entrained in glacial ice.

Nevertheless, the impact of surface runoff on regional TM concentrations is likely limited given that the submarine melting rate of 79NG is one order of magnitude larger than surface melt rates (Mayer et al., 2018). Approximately 90% of freshwater release from 79NG is through subglacial discharge and well below the surface layer with depths >90 m (Schaffer et al., 2020). In addition, the surface runoff is affected by seasonal variations with runoff only occurring during a narrow period in summer (Mankoff et al., 2020). In contrast, the inflow of AIW and basal ice melt of the floating ice tongue is a persistent feature occurring year round (Schaffer et al., 2020).

Therefore, when compared with submarine meltwater, surface runoff does not have a significant impact on biogeochemical cycles in this locality.

5.8. Toward a Mechanistic Understanding of Trace Metal Enrichment in Ice Shelf Outflow

Due to the obvious logistical difficulties, few cruises have been able to sample in close proximity to ice shelves and much of the available TM data for these environments is limited to Fe (e.g., Gerringa et al., 2012). In the absence of tracers of meltwater (such as ΔHe and Ra isotopic activities), unveiling the source of TMs at ice shelf stations is challenging, particularly around Antarctica where TM concentrations are generally lower than Arctic coastal waters (Marsay et al., 2017; Sherrell et al., 2015). Nevertheless, contrasting results herein with the best studied ice shelf proximal sites in the Amundsen and Ross Seas reveals some similarities.

Surface enrichments of dFe around Antarctica are sporadic and more often than not absent at proximal ice shelf stations compared to background concentrations (Marsay et al., 2017; Sherrell et al., 2015). Outflow from beneath the Dotson Ice Shelf illustrated dFe enrichment of 0.7 nM with enrichment also evident for dCu and dMn, but not for dNi (Sherrell et al., 2015). A pronounced surface enrichment of dMn was found up to concentrations of 6 nM (Sherrell et al., 2015; van Manen et al., 2022). Using a three-endmember mass balance approach, however, the contribution of ice melt to observed dFe concentrations in the Dotson Shelf outflow is deduced to be minor, ∼0.03 nM (van Manen et al., 2022). It is therefore indicated that most of these enrichments are not directly from basal ice melt, corroborating the hypothesis that dTM enrichments in cavity outflow may be primarily driven by sedimentary sources.

In the Ross Sea, surface dFe enrichment is also lacking close to the Ross Ice Shelf (Marsay et al., 2017), although slight enrichments of pFe (average 4.1 ± 1.2 nM) were found in the upper 100 m. The dFe concentrations in the ice shelf outflow were indistinguishable from other shelf stations. As per the Amundsen Sea (van Manen et al., 2022), pFe and pAl were significantly correlated, corroborating a lithogenic origin for most pFe. Elevated concentrations of pMn, pFe and pAl in nepheloid layers further suggested sediment resuspension as a major local driver of TM distributions (Marsay et al., 2017; Planquette et al., 2013). Similarly in austral autumn, Sedwick et al. (2022) found no clear evidence of dFe enrichments associated with ice melting. They did however discover similar distributions of dFe, pFe, pMn, and pAl, again supporting a major role for suspended sediment particles in regulating TM dynamics.

Together with the findings of our study, it is demonstrated that lithogenic particles are a major TM source driving pTM peaks. Most TMs present at elevated concentrations near ice shelves or glacier cavities do not appear to be directly sourced from basal ice melt. Specifically, for 79NG, it is only by considering multiple TM distributions alongside a water mass analysis and tracers of meltwater that the dominant roles of cavity overturning and sediment resuspension are revealed as major drivers of TM enrichments. Such subtleties have implications for how the associated TM fluxes are parameterized and are likely important considerations in realistically constraining the influence of ice shelves on marine TM dynamics (Dinniman et al., 2020).

6. Conclusions

We provided a comprehensive data set to illustrate the distributions of TMs in both dissolved and particulate phases on the NE Greenland shelf. Except for Cd, the assessed dTMs (dFe, dCo, dNi, dCu, and dMn) showed surface enrichment, ascribed to Arctic surface waters carried by the southbound TPD. Whilst dCu and dNi on the shelf appeared to have been relatively conservative during the lateral transportation of Arctic surface waters, dCo and dMn may have received additional inputs from local submarine melting of glacier ice. Submarine meltwater exiting the 79NG cavity, as distinguished by ΔHe, showed elevated dTM (Co, Cu, Fe, Mn, and Ni) concentrations. This observation can be ascribed to the equilibrium between dissolved and particulate materials from ice melt, inflowing AIW, and sediments in the cavity during the long residence time of AIW. Whilst the plume of dTMs emerges in mAIW at a depth of 70–100 m, a large plume of LpTMs TpTMs occurs at ∼200 m exiting the glacial cavity, ascribed to the re-suspension of cavity sediments. The correlations among LpTMs and TpTi, TpV, and TpAl demonstrate that most LpTMs in the cavity outflow were sourced from lithogenic particles. In contrast, the moderate correlation between LpCd and TpP is consistent with a more major role of biogenic particles for LpCd distributions.

The decoupling of subglacial dTM export from LpTMs supply was predominant in the subglacial discharge downstream to the 79NG terminus, although the overall LpTM-dTM dynamics on the NE Greenland shelf were mainly regulated by the relatively conservative mixing between LpTM-rich AIW and LpTM-poor Arctic surface waters. The LpTM plume from the 79NG cavity outflow may have contributed to elevated dTM concentrations (e.g., dCo and dMn) via particle dissolution as observed at downstream stations on the shelf (e.g., Dijmphna Sund). Our work is corroborated by previous findings from ice shelves around Antarctica, that suggest LpTMs and dFe enrichments near ice shelves are mainly supplied by sedimentary sources rather than directly by ice melting.

Conflict of Interest

The authors declare no conflicts of interest relevant to this study.

Data Availability Statement

All data used to support the findings of this work are accessible from Pangaea oceanographic repository with the following links: Physical oceanography data (ucCTD stations): https://doi.pangaea.de/10.1594/PANGAEA.871030 (Kanzow et al., 2017b). Physical oceanography data (lvCTD stations): https://doi.pangaea.de/10.1594/PANGAEA.871028 (Kanzow et al., 2017a). Macronutrient data (ucCTD stations): https://doi.pangaea.de/10.1594/PANGAEA.905347 (Graeve et al., 2019). Dissolved trace elements (ucCTD stations): https://doi.pangaea.de/10.1594/PANGAEA.933431 (Krisch, Roig, et al., 2021). Labile, particulate, and labile fraction data for trace elements (ucCTD stations): https://doi.pangaea.de/10.1594/PANGAEA.948466 (Al-Hashem, Achterberg, et al., 2022). Radium isotope data (lvCTD stations): https://doi.pangaea.de/10.1594/PANGAEA.936029 and https://doi.pangaea.de/10.1594/PANGAEA.936027 (Rutgers van der Loeff et al., 2021a, 2021b). Noble gas data (lvCTD stations): https://doi.org/10.1594/PANGAEA.931336 (Huhn, Rhein, Bulsiewicz, & Sültenfuß, 2021). Stable oxygen isotope data (lvCTD stations): https://doi.pangaea.de/10.1594/PANGAEA.927429 (Meyer et al., 2021).

Acknowledgments
The authors thank chief scientists Torsten Kanzow (GN05/PS100), captain Schwarze and the crew of the RV Polarstern, operated by the Alfred Wegener Institute, Helmholtz Centre for Polar and Marine Research (AWI). The PhD fellowships to A. Al-Hashem and S. Krisch were funded by the Kuwait Institute for Scientific Research, Kuwait, and the Deutsche Forschungsgemeinschaft (AC 217/1-1 granted to Eric P. Achterberg), respectively. Mark J. Hopwood was financed by the DFG (Award HO 6321/1-1). Open Access funding enabled and organized by Projekt DEAL.

References

Aagaard, K., & Carmack, E. C. (1989). The role of sea ice and other fresh water in the Arctic circulation. *Journal of Geophysical Research*, *94*(C10), 14485–14498. https://doi.org/10.1029/jc094ic10p14485

Achterberg, E. P., Steigenberger, S., Klar, J. K., Browning, T. J., Marsay, C. M., Painter, S. C., et al. (2021). Trace element biogeochemistry in the high-latitude North Atlantic Ocean: Seasonal variations and volcanic inputs. *Global Biogeochemical Cycles*, *35*(3), e2020GB006674. https://doi.org/10.1029/2020GB006674

Al-Hashem, A. A., Achterberg, E. P., Krisch, S., Lodeiro, P. F., & Chen, X.-G. (2022). Particulate trace elements (Al, Ti, V, P, Fe, Mn, Co, Ni, Cu, and Cd) measured on water bottle samples from ultra clean CTD/Water sampler-system during POLARSTERN cruise PS100/GN05 [Dataset]. PANGAEA. Retrieved from https://doi.pangaea.de/10.1594/PANGAEA.948466

Al-Hashem, A. A., Beck, A. J., Krisch, S., Menzel Barraqueta, J.-L., Steffens, T., & Achterberg, E. P. (2022). Particulate trace metal sources, cycling, and distributions on the southwest African shelf. *Global Biogeochemical Cycles*, *36*(11), e2022GB007453. https://doi.org/10.1029/2022GB007453

An, L., Rignot, E., Wood, M., Willis, J. K., Mouginot, J., & Khan, S. A. (2021). Ocean melting of the Zachariae Isstrom and Nioghalvfjerdsfjorden glaciers, northeast Greenland. *Proceedings of the National Academy of Sciences of the United States of America*, *118*(2), e2015483118. https://doi.org/10.1073/pnas.2015483118

Aphalo, P. J. (2022). ggpmisc: Miscellaneous Extensions to "ggplot2. Retrieved from https://docs.r4photobiology.info/ggpmisc/

Ardiningsih, I., Krisch, S., Lodeiro, P., Reichart, G.-J., Achterberg, E. P., Gledhill, M., et al. (2020). Natural Fe-binding organic ligands in Fram Strait and over the Northeast Greenland shelf. *Marine Chemistry*, *224*, 103815. https://doi.org/10.1016/j.marchem.2020.103815

Arndt, J. E., Jokat, W., Dorschel, B., Myklebust, R., Dowdeswell, J. A., & Evans, J. (2015). A new bathymetry of the Northeast Greenland continental shelf: Constraints on glacial and other processes. *Geochemistry, Geophysics, Geosystems*, *16*(10), 3733–3753. https://doi.org/10.1002/2015GC005931

Azetsu-Scott, K., & Tan, F. C. (1997). Oxygen isotope studies from Iceland to an East Greenland Fjord: Behaviour of glacial meltwater plume. *Marine Chemistry*, *56*(3–4), 239–251. https://doi.org/10.1016/s0304-4203(96)00078-3

Baeyens, W., Bowie, A. R., Buesseler, K., Elskens, M., Gao, Y., Lamborg, C., et al. (2011). Size-fractionated labile trace elements in the Northwest Pacific and southern oceans. *Marine Chemistry*, *126*(1), 108–113. https://doi.org/10.1016/j.marchem.2011.04.004

Barrett, P. M., Resing, J. A., Grand, M. M., Measures, C. I., & Landing, W. M. (2018). Trace element composition of suspended particulate matter along three meridional CLIVAR sections in the Indian and Southern Oceans: Impact of scavenging on Al distributions. *Chemical Geology*, *502*, 15–28. https://doi.org/10.1016/j.chemgeo.2018.06.015

Bauch, D., van der Loeff, M. R., Andersen, N., Torres-Valdes, S., Bakker, K., & Abrahamsen, E. P. (2011). Origin of freshwater and polynya water in the Arctic Ocean halocline in summer 2007. *Progress in Oceanography*, *91*(4), 482–495. https://doi.org/10.1016/j.pocean.2011.07.017

Beaird, N., Straneo, F., & Jenkins, W. (2015). Spreading of Greenland meltwaters in the ocean revealed by noble gases. *Geophysical Research Letters*, *42*(18), 7705–7713. https://doi.org/10.1002/2015GL065003

Behrenfeld, M. J., & Kolber, Z. S. (1999). Widespread iron limitation of phytoplankton in the South Pacific Ocean. *Science*, *283*(5403), 840–843. https://doi.org/10.1126/science.283.5403.840

Berger, C. J. M., Lippiatt, S. M., Lawrence, M. G., & Bruland, K. W. (2008). Application of a chemical leach technique for estimating labile particulate aluminum, iron, and manganese in the Columbia River plume and coastal waters off Oregon and Washington. *Journal of Geophysical Research*, *113*(C2), C00B01. https://doi.org/10.1029/2007JC004703

Bourke, R. H., Newton, J. L., Paquette, R. G., & Tunnicliffe, M. D. (1987). Circulation and water masses of the East Greenland shelf. *Journal of Geophysical Research*, *92*(C7), 6729–6740. https://doi.org/10.1029/JC092iC07p06729

Boyle, E. A., Sclater, F., & Edmond, J. M. (1976). On the marine geochemistry of cadmium. *Nature*, *263*(5572), 42–44. https://doi.org/10.1038/263042a0

Browning, T. J., Achterberg, E. P., Engel, A., & Mawji, E. (2021). Manganese co-limitation of phytoplankton growth and major nutrient drawdown in the Southern Ocean. *Nature Communications*, *12*(1), 884. https://doi.org/10.1038/s41467-021-21122-6

Browning, T. J., Liu, X., Zhang, R., Wen, Z., Liu, J., Zhou, Y., et al. (2022). Nutrient co-limitation in the subtropical Northwest Pacific. *Limnology and Oceanography Letters*, *7*(1), 52–61. https://doi.org/10.1002/lol2.10205

Bundy, R. M., Tagliabue, A., Hawco, N. J., Morton, P. L., Twining, B. S., Hatta, M., et al. (2020). Elevated sources of cobalt in the Arctic Ocean. *Biogeosciences*, *17*(19), 4745–4767. https://doi.org/10.5194/bg-17-4745-2020

Cape, M. R., Straneo, F., Beaird, N., Bundy, R. M., & Charette, M. A. (2019). Nutrient release to oceans from buoyancy-driven upwelling at Greenland tidewater glaciers. *Nature Geoscience*, *12*(1), 34–39. https://doi.org/10.1038/s41561-018-0268-4

Charette, M. A., Kipp, L. E., Jensen, L. T., Dabrowski, J. S., Whitmore, L. M., Fitzsimmons, J. N., et al. (2020). The transpolar drift as a source of riverine and shelf-derived trace elements to the central Arctic Ocean. *Journal of Geophysical Research: Oceans*, *125*(5), e2019JC015920. https://doi.org/10.1029/2019JC015920

Charette, M. A., Lam, P. J., Lohan, M. C., Kwon, E. Y., Hatje, V., Jeandel, C., et al. (2016). Coastal ocean and shelf-sea biogeochemical cycling of trace elements and isotopes: Lessons learned from GEOTRACES. *Philosophical Transactions of the Royal Society A: Mathematical, Physical & Engineering Sciences*, *374*(2081), 20160076. https://doi.org/10.1098/rsta.2016.0076

Cullen, J. T., & Sherrell, R. M. (1999). Techniques for determination of trace metals in small samples of size-fractionated particulate matter: Phytoplankton metals off central California. *Marine Chemistry*, *67*(3–4), 233–247. https://doi.org/10.1016/s0304-4203(99)00060-2

Cutter, G., Casciotti, K., Croot, P., Geibert, W., Heimbürger, L.-E., Lohan, M., et al. (2017). *Sampling and sample-handling protocols for GEOTRACES cruises*. GEOTRACES Standards and Intercalibration Committee.

Dai, M.-H., & Martin, J.-M. (1995). First data on trace metal level and behaviour in two major Arctic river-estuarine systems (Ob and Yenisey) and in the adjacent Kara Sea, Russia. *Earth and Planetary Science Letters*, *131*(3), 127–141. https://doi.org/10.1016/0012-821X(95)00021-4

de Steur, L., Hansen, E., Mauritzen, C., Beszczynska-Möller, A., & Fahrbach, E. (2014). Impact of recirculation on the East Greenland Current in Fram Strait: Results from moored current meter measurements between 1997 and 2009. *Deep Sea Research Part I: Oceanographic Research Papers*, *92*, 26–40. https://doi.org/10.1016/j.dsr.2014.05.018

de Steur, L., Peralta-Ferriz, C., & Pavlova, O. (2018). Freshwater export in the East Greenland Current freshens the North Atlantic. *Geophysical Research Letters*, *45*(24), 13359–13366. https://doi.org/10.1029/2018GL080207

Dinniman, M. S., St-Laurent, P., Arrigo, K. R., Hofmann, E. E., & van Dijken, G. L. (2020). Analysis of iron sources in Antarctic continental shelf waters. *Journal of Geophysical Research: Oceans*, *125*(5), e2019JC015736. https://doi.org/10.1029/2019JC015736

Fahrbach, E., Meincke, J., Østerhus, S., Rohardt, G., Schauer, U., Tverberg, V., & Verduin, J. (2001). Direct measurements of volume transports through Fram Strait. *Polar Research*, *20*(2), 217–224. https://doi.org/10.1111/j.1751-8369.2001.tb00059.x

Gerringa, L. J. A., Alderkamp, A.-C., Laan, P., Thuroczy, C.-E., De Baar, H. J., Mills, M. M., et al. (2012). Iron from melting glaciers fuels the phytoplankton blooms in Amundsen Sea (Southern Ocean): Iron biogeochemistry. *Deep Sea Research Part II: Topical Studies in Oceanography*, *71*, 16–31. https://doi.org/10.1016/j.dsr2.2012.03.007

Gerringa, L. J. A., Rijkenberg, M. J. A., Slagter, H. A., Laan, P., Paffrath, R., Bauch, D., et al. (2021). Dissolved Cd, Co, Cu, Fe, Mn, Ni, and Zn in the Arctic Ocean. *Journal of Geophysical Research: Oceans*, *126*(9), e2021JC017323. https://doi.org/10.1029/2021JC017323

Gordeev, V. V. (2000). River input of water, sediment, major ions, nutrients and trace metals from Russian territory to the Arctic Ocean. In E. L. Lewis, E. P. Jones, P. Lemke, T. D. Prowse, & P. Wadhams (Eds.), *The freshwater budget of the Arctic Ocean* (pp. 297–322). Springer Netherlands. https://doi.org/10.1007/978-94-011-4132-1_14

Graeve, M., Ludwichowski, K.-U., & Krisch, S. (2019). Inorganic nutrients measured on water bottle samples from ultra clean CTD/Water sampler-system during POLARSTERN cruise PS100 (ARK-XXX/2), version 2 [Dataset]. Alfred Wegener Institute, Helmholtz Centre for Polar and Marine Research. PANGAEA. https://doi.org/10.1594/PANGAEA.905347

Guieu, C., Huang, W. W., Martin, J.-M., & Yong, Y. Y. (1996). Outflow of trace metals into the Laptev Sea by the Lena River. *Marine Chemistry*, *53*(3), 255–267. https://doi.org/10.1016/0304-4203(95)00093-3

Hohmann, R., Schlosser, P., Jacobs, S., Ludin, A., & Weppernig, R. (2002). Excess helium and neon in the southeast Pacific: Tracers for glacial meltwater. *Journal of Geophysical Research*, *107*(C11), 19-1–19-14. https://doi.org/10.1029/2000JC000378

Homoky, W. B., Severmann, S., McManus, J., Berelson, W. M., Riedel, T. E., Statham, P. J., & Mills, R. A. (2012). Dissolved oxygen and suspended particles regulate the benthic flux of iron from continental margins. *Marine Chemistry*, *134*, 59–70. https://doi.org/10.1016/j.marchem.2012.03.003

Honeyman, B. D., Balistrieri, L. S., & Murray, J. W. (1988). Oceanic trace metal scavenging: The importance of particle concentration. *Deep-Sea Research, Part A: Oceanographic Research Papers*, *35*(2), 227–246. https://doi.org/10.1016/0198-0149(88)90038-6

Huhn, O., Rhein, M., Bulsiewicz, K., & Sültenfuß, J. (2021). Noble gas (He, Ne isotopes) and transient tracer (CFC-11 and CFC-12) measurements from POLARSTERN cruise PS100 (northeast Greenland, 2016) [Dataset]. PANGAEA. https://doi.org/10.1594/PANGAEA.931336

Huhn, O., Rhein, M., Kanzow, T., Schaffer, J., & Sültenfuß, J. (2021). Submarine meltwater from Nioghalvfjerdsbræ (79 north Glacier), northeast Greenland. *Journal of Geophysical Research: Oceans*, *126*(7), e2021JC017224. https://doi.org/10.1029/2021JC017224

Kandel, A., & Aguilar-Islas, A. (2021). Spatial and temporal variability of dissolved aluminum and manganese in surface waters of the northern Gulf of Alaska. *Deep Sea Research Part II: Topical Studies in Oceanography*, *189–190*, 104952. https://doi.org/10.1016/j.dsr2.2021.104952

Kanna, N., Sugiyama, S., Fukamachi, Y., Nomura, D., & Nishioka, J. (2020). Iron supply by subglacial discharge into a fjord near the front of a marine-terminating glacier in northwestern Greenland. *Global Biogeochemical Cycles*, *34*(10), e2020GB006567. https://doi.org/10.1029/2020GB006567

Kanzow, T., von Appen, W.-J., Schaffer, J., Köhn, E., Tsubouchi, T., Wilson, N., et al. (2017b). Physical oceanography measured with ultra clean CTD/water sampler-system during POLARSTERN cruise PS100 (ARK-XXX/2) [Dataset]. Alfred Wegener Institute, Helmholtz Centre for Polar and Marine Research. PANGAEA. https://doi.org/10.1594/PANGAEA.871030

Kanzow, T., von Appen, W.-J., Schaffer, J., Köhn, E., Tsubouchi, T., Wilson, N., & Wisotzki, A. (2017a). Physical oceanography measured on water bottle samples from CTD/Large volume Watersampler-system during POLARSTERN cruise PS100 (ARK-XXX/2) [Dataset]. Alfred Wegener Institute, Helmholtz Centre for Polar and Marine Research. PANGAEA. https://doi.org/10.1594/PANGAEA.871028

Kim, I., Hahm, D., Rhee, T. S., Kim, T. W., Kim, C.-S., & Lee, S. (2016). The distribution of glacial meltwater in the Amundsen Sea, Antarctica, revealed by dissolved helium and neon. *Journal of Geophysical Research: Oceans*, *121*(3), 1654–1666. https://doi.org/10.1002/2015JC011211

Kipp, L. E., Charette, M. A., Moore, W. S., Henderson, P. B., & Rigor, I. G. (2018). Increased fluxes of shelf-derived materials to the central Arctic Ocean. *Science Advances*, *4*(1), eaao1302. https://doi.org/10.1126/sciadv.aao1302

Krause, J., Hopwood, M. J., Höfer, J., Krisch, S., Achterberg, E. P., Alarcón, E., et al. (2021). Trace element (Fe, Co, Ni and Cu) dynamics across the salinity Gradient in Arctic and Antarctic glacier fjords. *Frontiers of Earth Science*, *9*, 878. https://doi.org/10.3389/feart.2021.725279

Krisch, S., Browning, T. J., Graeve, M., Ludwichowski, K.-U., Lodeiro, P., Hopwood, M. J., et al. (2020). The influence of Arctic Fe and Atlantic fixed N on summertime primary production in Fram Strait, North Greenland Sea. *Scientific Reports*, *10*(1), 15230. https://doi.org/10.1038/s41598-020-72100-9

Krisch, S., Hopwood, M. J., Roig, S., Gerringa, L. J. A., Middag, R., Rutgers van der Loeff, M. M., et al. (2022). Arctic–Atlantic exchange of the dissolved micronutrients iron, manganese, cobalt, nickel, copper and zinc with a focus on Fram Strait. *Global Biogeochemical Cycles*, *36*(5), e2021GB007191. https://doi.org/10.1029/2021GB007191

Krisch, S., Hopwood, M. J., Schaffer, J., Al-Hashem, A., Höfer, J., Rutgers van der Loeff, M. M., et al. (2021). The 79°N Glacier cavity modulates subglacial iron export to the NE Greenland shelf. *Nature Communications*, *12*(1), 3030. https://doi.org/10.1038/s41467-021-23093-0

Krisch, S., Huhn, O., Al-Hashem, A., Hopwood, M. J., Lodeiro, P., & Achterberg, E. P. (2022). Quantifying ice-sheet derived lean (Pb) fluxes to the ocean; a case study at Nioghalvfjerdsbrae. *Geophysical Research Letters*, *49*(21), e2022GL100296. https://doi.org/10.1029/2022GL100296

Krisch, S., Roig, S., Lodeiro, P. F., Yong, J.-C., Herzberg, N., Evers, F., et al. (2021). Dissolved trace elements (Fe, Mn, Co, Ni, Cu, Zn, Cd and Pb) measured on water bottle samples from ultra clean CTD/water sampler-system during POLARSTERN cruise PS100/GN05 (ARK-XXX/2) [Dataset]. PANGAEA. Retrieved from https://doi.pangaea.de/10.1594/PANGAEA.933431

Lara, R. J., Kattner, G., Tillmann, U., & Hirche, H.-J. (1994). The North East water polynya (Greenland Sea). *Polar Biology*, *14*(7), 483–490. https://doi.org/10.1007/BF00239053

Laukert, G., Frank, M., Bauch, D., Hathorne, E. C., Rabe, B., von Appen, W.-J., et al. (2017). Ocean circulation and freshwater pathways in the Arctic Mediterranean based on a combined Nd isotope, REE and oxygen isotope section across Fram Strait. *Geochimica et Cosmochimica Acta*, *202*, 285–309. https://doi.org/10.1016/j.gca.2016.12.028

Lippiatt, S. M., Lohan, M. C., & Bruland, K. W. (2010). The distribution of reactive iron in northern Gulf of Alaska coastal waters. *Marine Chemistry*, *121*(1–4), 187–199. https://doi.org/10.1016/j.marchem.2010.04.007

Lohan, M. C., & Tagliabue, A. (2018). Oceanic micronutrients: Trace metals that are essential for marine life. *Elements*, *14*(6), 385–390. https://doi.org/10.2138/gselements.14.6.385

Loose, B., & Jenkins, W. J. (2014). The five stable noble gases are sensitive unambiguous tracers of glacial meltwater. *Geophysical Research Letters*, *41*(8), 2835–2841. https://doi.org/10.1002/2013GL058804

Mankoff, K. D., Solgaard, A., Colgan, W., Ahlstrøm, A. P., Khan, S. A., & Fausto, R. S. (2020). Greenland Ice Sheet solid ice discharge from 1986 through March 2020. *Earth System Science Data*, *12*(2), 1367–1383. https://doi.org/10.5194/essd-12-1367-2020

Marsay, C. M., Barrett, P. M., McGillicuddy, D. J., Jr., & Sedwick, P. N. (2017). Distributions, sources, and transformations of dissolved and particulate iron on the Ross Sea continental shelf during summer. *Journal of Geophysical Research: Oceans*, *122*(8), 6371–6393. https://doi.org/10.1002/2017JC013068

Mayer, C., Reeh, N., Jung-Rothenhausler, F., Huybrechts, P., & Oerter, H. (2000). The subglacial cavity and implied dynamics under Nioghalvfjerdsfjorden glacier, NE-Greenland. *Geophysical Research Letters*, *27*(15), 2289–2292. https://doi.org/10.1029/2000GL011514

Mayer, C., Schaffer, J., Hattermann, T., Floricioiu, D., Krieger, L., Dodd, P. A., et al. (2018). Large ice loss variability at Nioghalvfjerdsfjorden glacier, northeast-Greenland. *Nature Communications*, *9*(1), 2768. https://doi.org/10.1038/s41467-018-05180-x

Meire, L., Meire, P., Struyf, E., Krawczyk, D. W., Arendt, K. E., Yde, J. C., et al. (2016). High export of dissolved silica from the Greenland Ice Sheet. *Geophysical Research Letters*, *43*(17), 9173–9182. https://doi.org/10.1002/2016GL070191

Menzel Barraqueta, J.-L., Schlosser, C., Planquette, H., Gourain, A., Cheize, M., Boutorh, J., et al. (2018). Aluminium in the North Atlantic Ocean and the Labrador Sea (GEOTRACES GA01 section): Roles of continental inputs and biogenic particle removal. *Biogeosciences*, *15*(16), 5271–5286. https://doi.org/10.5194/bg-15-5271-2018

Meyer, H., Schaffer, J., Rabe, B., & Rutgers van der Loeff, M. M. (2021). Oxygen and hydrogen isotopes in water samples collected during Polarstern cruise PS100 in 2016 [Dataset]. PANGAEA. https://doi.org/10.1594/PANGAEA.927429

Meyer, H., Schönicke, L., Wand, U., Hubberten, H. W., & Friedrichsen, H. (2000). Isotope studies of hydrogen and oxygen in ground ice – Experiences with the equilibration technique. *Isotopes in Environmental and Health Studies*, *36*(2), 133–149. https://doi.org/10.1080/10256010008032939

Moore, C. M., Mills, M. M., Arrigo, K. R., Berman-Frank, I., Bopp, L., Boyd, P. W., et al. (2013). Processes and patterns of oceanic nutrient limitation. *Nature Geoscience*, *6*(9), 701–710. https://doi.org/10.1038/ngeo1765

Moore, W. S. (2000). Determining coastal mixing rates using radium isotopes. *Continental Shelf Research*, *20*(15), 1993–2007. https://doi.org/10.1016/S0278-4343(00)00054-6

Morel, F. M. M., & Price, N. M. (2003). The biogeochemical cycles of trace metals in the oceans. *Science*, *300*(5621), 944–947. https://doi.org/10.1126/science.1083545

Mouginot, J., Rignot, E., Scheuchl, B., Fenty, I., Khazendar, A., Morlighem, M., et al. (2015). Fast retreat of Zachariæ Isstrøm, northeast Greenland. *Science*, *350*(6266), 1357–1361. https://doi.org/10.1126/science.aac7111

NASA. (2022). Greenland's Spalte glacier disintegrates. Retrieved from https://climate.nasa.gov/images-of-change?id=752

Panzeca, C., Beck, A. J., Leblanc, K., Taylor, G. T., Hutchins, D. A., & Sañudo-Wilhelmy, S. A. (2008). Potential cobalt limitation of vitamin B12 synthesis in the North Atlantic Ocean. *Global Biogeochemical Cycles*, *22*(2), GB2029. https://doi.org/10.1029/2007GB003124

Paulsen, M. L., Nielsen, S. E. B., Müller, O., Møller, E. F., Stedmon, C. A., Juul-Pedersen, T., et al. (2017). Carbon bioavailability in a high Arctic fjord influenced by Glacial meltwater, NE Greenland. *Frontiers in Marine Science*, *4*, 176. https://doi.org/10.3389/fmars.2017.00176

Pesant, S., Legendre, L., Gosselin, M., Ashjian, C., Booth, B., Daly, K., et al. (1998). Pathways of carbon cycling in the euphotic zone: The fate of largesized phytoplankton in the Northeast water polynya. *Journal of Plankton Research*, *20*(7), 1267–1291. https://doi.org/10.1093/plankt/20.7.1267

Planquette, H., Sherrell, R. M., Stammerjohn, S., & Field, M. P. (2013). Particulate iron delivery to the water column of the Amundsen Sea, Antarctica. *Marine Chemistry*, *153*, 15–30. https://doi.org/10.1016/j.marchem.2013.04.006

Price, N. M., & Morel, F. M. M. (1991). Colimitation of phytoplankton growth by nickel and nitrogen. *Limnology & Oceanography*, *36*(6), 1071–1077. https://doi.org/10.4319/lo.1991.36.6.1071

Rapp, I., Schlosser, C., Rusiecka, D., Gledhill, M., & Achterberg, E. P. (2017). Automated preconcentration of Fe, Zn, Cu, Ni, Cd, Pb, Co, and Mn in seawater with analysis using high-resolution sector field inductively-coupled plasma mass spectrometry. *Analytica Chimica Acta*, *976*, 1–13. https://doi.org/10.1016/j.aca.2017.05.008

Revelle, W. R. (2017). psych: Procedures for personality and psychological research. Software.

Rhein, M., Steinfeldt, R., Huhn, O., Sültenfuß, J., & Breckenfelder, T. (2018). Greenland submarine melt water observed in the Labrador and Irminger Sea. *Geophysical Research Letters*, *45*(19), 10570–10578. https://doi.org/10.1029/2018GL079110

Richter, M. E., von Appen, W.-J., & Wekerle, C. (2018). Does the East Greenland Current exist in the northern Fram Strait? *Ocean Science*, *14*(5), 1147–1165. https://doi.org/10.5194/os-14-1147-2018

Rignot, E., & Mouginot, J. (2012). Ice flow in Greenland for the International polar year 2008–2009. *Geophysical Research Letters*, *39*(11). https://doi.org/10.1029/2012GL051634

Rudels, B., Björk, G., Nilsson, J., Winsor, P., Lake, I., & Nohr, C. (2005). The interaction between waters from the Arctic Ocean and the Nordic Seas north of Fram Strait and along the East Greenland Current: Results from the Arctic Ocean-02 Oden expedition. *Journal of Marine Systems*, *55*(1–2), 1–30. https://doi.org/10.1016/j.jmarsys.2004.06.008

Rudnick, R. L., & Gao, S. (2003). 3.01 Composition of the continental crust. In *The crust*. Elsevier-Pergamon. https://doi.org/10.1016/B0-08-043751-6/03016-4

Rutgers van der Loeff, M. M., Cai, P., Stimac, I., Bauch, D., Hanfland, C., Roeske, T., & Moran, S. B. (2012). Shelf-basin exchange times of Arctic surface waters estimated from ^{228}Th/^{228}Ra disequilibrium. *Journal of Geophysical Research*, *117*(C3). https://doi.org/10.1029/2011JC007478

Rutgers van der Loeff, M. M., Kipp, L., Charette, M. A., Moore, W. S., Black, E., Stimac, I., et al. (2018). Radium isotopes across the Arctic Ocean show time scales of water mass ventilation and increasing shelf inputs. *Journal of Geophysical Research: Oceans*, *123*(7), 4853–4873. https://doi.org/10.1029/2018JC013888

Rutgers van der Loeff, M. M., Stimac, I., Valk, O., Geibert, W., & Vieira, L. H. (2021a). Radium isotopes and ^{228}Th in surface water samples collected on POLARSTERN expedition PS100 [Dataset]. PANGAEA. Retrieved from https://doi.pangaea.de/10.1594/PANGAEA.936029

Rutgers van der Loeff, M. M., Stimac, I., Valk, O., Geibert, W., & Vieira, L. H. (2021b). Radium isotopes and ^{228}Th in water column samples collected on POLARSTERN expedition PS100 [Dataset]. PANGAEA. Retrieved from https://doi.pangaea.de/10.1594/PANGAEA.936027

Schaffer, J., Kanzow, T., von Appen, W.-J., von Albedyll, L., Arndt, J. E., & Roberts, D. H. (2020). Bathymetry constrains ocean heat supply to Greenland's largest glacier tongue. *Nature Geoscience*, *13*(3), 227–231. https://doi.org/10.1038/s41561-019-0529-x

Schaffer, J., von Appen, W.-J., Dodd, P. A., Hofstede, C., Mayer, C., de Steur, L., & Kanzow, T. (2017). Warm water pathways toward Nioghalvfjerdsfjorden Glacier, Northeast Greenland. *Journal of Geophysical Research: Oceans*, *122*(5), 4004–4020. https://doi.org/10.1002/2016JC012462

Schlitzer, R. (2021). Ocean Data View. Retrieves from https://odv.awi.de/

Sedwick, P. N., Sohst, B. M., O'Hara, C., Stammerjohn, S. E., Loose, B., Dinniman, M. S., et al. (2022). Seasonal dynamics of dissolved iron on the Antarctic continental shelf: Late-fall observations from the Terra Nova Bay and Ross Ice Shelf polynyas. *Journal of Geophysical Research: Oceans*, *127*(10), e2022JC018999. https://doi.org/10.1029/2022JC018999

Sherrell, R. M., Lagerström, M. E., Forsch, K. O., Stammerjohn, S. E., & Yager, P. L. (2015). Dynamics of dissolved iron and other bioactive trace metals (Mn, Ni, Cu, Zn) in the Amundsen Sea Polynya, Antarctica. *Elementa: Science of the Anthropocene*, *3*, 000071. https://doi.org/10.12952/journal.elementa.000071

Sholkovitz, E. R. (1978). The flocculation of dissolved Fe, Mn, Al, Cu, Ni, Co and Cd during estuarine mixing. *Earth and Planetary Science Letters*, *41*(1), 77–86. https://doi.org/10.1016/0012-821X(78)90043-2

Slagter, H. A., Reader, H. E., Rijkenberg, M. J. A., Rutgers van der Loeff, M., de Baar, H. J. W., & Gerringa, L. J. A. (2017). Organic Fe speciation in the Eurasian basins of the Arctic Ocean and its relation to terrestrial DOM. *Marine Chemistry*, *197*, 11–25. https://doi.org/10.1016/j.marchem.2017.10.005

Stevenson, E. I., Fantle, M. S., Das, S. B., Williams, H. M., & Aciego, S. M. (2017). The iron isotopic composition of subglacial streams draining the Greenland ice sheet. *Geochimica et Cosmochimica Acta*, *213*, 237–254. https://doi.org/10.1016/j.gca.2017.06.002

Sültenfuß, J., Roether, W., & Rhein, M. (2009). The Bremen mass spectrometric facility for the measurement of helium isotopes, neon, and tritium in water. *Isotopes in Environmental and Health Studies*, *45*(2), 83–95. https://doi.org/10.1080/10256010902871929

Sunda, W. G., & Huntsman, S. A. (1988). Effect of sunlight on redox cycles of manganese in the southwestern Sargasso Sea. *Deep-Sea Research, Part A: Oceanographic Research Papers*, *35*(8), 1297–1317. https://doi.org/10.1016/0198-0149(88)90084-2

Sunda, W. G., Huntsman, S. A., & Harvey, G. R. (1983). Photoreduction of manganese oxides in seawater and its geochemical and biological implications. *Nature*, *301*(5897), 234–236. https://doi.org/10.1038/301234a0

Tiwari, M., Nagoji, S., Kumar, V., Tripathi, S., & Behera, P. (2018). Oxygen isotope-salinity relation in an Arctic fjord (Kongsfjorden): Implications to hydrographic variability. *Geoscience Frontiers*, *9*(6), 1937–1943. https://doi.org/10.1016/j.gsf.2017.12.007

Tonnard, M., Planquette, H., Bowie, A. R., Van Der Merwe, P., Gallinari, M., Desprez de Gésincourt, F., et al. (2020). Dissolved iron in the North Atlantic Ocean and Labrador Sea along the GEOVIDE section (GEOTRACES section GA01). *Biogeosciences*, *17*(4), 917–943. https://doi.org/10.5194/bg-17-917-2020

Torres-Valdés, S., Tsubouchi, T., Bacon, S., Naveira-Garabato, A. C., Sanders, R., McLaughlin, F. A., et al. (2013). Export of nutrients from the Arctic Ocean. *Journal of Geophysical Research: Oceans*, *118*(4), 1625–1644. https://doi.org/10.1002/jgrc.20063

Tovar-Sánchez, A., Duarte, C. M., Alonso, J. C., Lacorte, S., Tauler, R., & Galbán-Malagón, C. (2010). Impacts of metals and nutrients released from melting multiyear Arctic Sea ice. *Journal of Geophysical Research*, *115*(C7), C07003. https://doi.org/10.1029/2009JC005685

Tsubouchi, T., Bacon, S., Aksenov, Y., Garabato, A. C. N., Beszczynska-Möller, A., Hansen, E., et al. (2018). The Arctic Ocean seasonal cycles of heat and freshwater fluxes: Observation-based Inverse estimates. *Journal of Physical Oceanography*, *48*(9), 2029–2055. https://doi.org/10.1175/JPO-D-17-0239.1

Tuerena, R. E., Hopkins, J., Buchanan, P. J., Ganeshram, R. S., Norman, L., von Appen, W.-J., et al. (2021). An Arctic strait of two halves: The changing dynamics of nutrient uptake and limitation across the Fram Strait. *Global Biogeochemical Cycles*, *35*(9), e2021GB006961. https://doi.org/10.1029/2021GB006961

Twining, B. S., & Baines, S. B. (2013). The trace metal composition of marine phytoplankton. *Annual Review of Marine Science*, *5*(1), 191–215. https://doi.org/10.1146/annurev-marine-121211-172322

Twining, B. S., Rauschenberg, S., Morton, P. L., & Vogt, S. (2015). Metal contents of phytoplankton and labile particulate material in the North Atlantic Ocean. *Progress in Oceanography*, *137*, 261–283. https://doi.org/10.1016/j.pocean.2015.07.001

van Genuchten, C. M., Hopwood, M. J., Liu, T., Krause, J., Achterberg, E. P., Rosing, M. T., & Meire, L. (2022). Solid-phase Mn speciation in suspended particles along meltwater-influenced fjords of West Greenland. *Geochimica et Cosmochimica Acta*, *326*, 180–198. https://doi.org/10.1016/j.gca.2022.04.003

van Manen, M., Aoki, S., Brussaard, C. P. D., Conway, T. M., Eich, C., Gerringa, L. J. A., et al. (2022). The role of the Dotson Ice Shelf and Circumpolar Deep Water as driver and source of dissolved and particulate iron and manganese in the Amundsen Sea polynya, southern ocean. *Marine Chemistry*, *246*, 104161. https://doi.org/10.1016/j.marchem.2022.104161

von Albedyll, L., Schaffer, J., & Kanzow, T. (2021). Ocean variability at Greenland's largest glacier tongue linked to continental shelf circulation. *Journal of Geophysical Research: Oceans*, *126*(5), e2020JC017080. https://doi.org/10.1029/2020JC017080

Wickham, H., Averick, M., Bryan, J., Chang, W., McGowan, L. D., François, R., et al. (2019). Welcome to the tidyverse. *Journal of Open Source Software*, *4*(43), 1686. https://doi.org/10.21105/joss.01686

Wilson, N. J., & Straneo, F. (2015). Water exchange between the continental shelf and the cavity beneath Nioghalvfjerdsbrae (79 North Glacier). *Geophysical Research Letters*, *42*(18), 7648–7654. https://doi.org/10.1002/2015GL064944

Xu, Y., & Morel, F. M. M. (2013). Cadmium in marine phytoplankton. In A. Sigel, H. Sigel, & R. K. Sigel (Eds.), *Cadmium: From toxicity to essentiality* (pp. 509–528). Springer Netherlands. https://doi.org/10.1007/978-94-007-5179-8_16

Zhang, J. (1995). Geochemistry of trace metals from Chinese river/Estuary systems: An overview. *Estuarine, Coastal and Shelf Science*, *41*(6), 631–658. https://doi.org/10.1006/ecss.1995.0082

Zhang, R., Jensen, L. T., Fitzsimmons, J. N., Sherrell, R. M., & John, S. (2019). Dissolved cadmium and cadmium stable isotopes in the western Arctic Ocean. *Geochimica et Cosmochimica Acta*, *258*, 258–273. https://doi.org/10.1016/j.gca.2019.05.028

References From the Supporting Information

Cullen, J. T., Field, M. P., & Sherrell, R. M. (2001). Determination of trace elements in filtered suspended marine particulate material by sector field HR-ICP-MS. *Journal of Analytical Atomic Spectrometry*, *16*(11), 1307–1312. https://doi.org/10.1039/B104398F

Grasshoff, K., Kremlingl, K., & Ehrhardt, M. (1999). *Methods of seawater analysis* (3rd ed.). WILEY-VCH Verlag GmbH. https://doi.org/10.1002/9783527613984

Jochum, K. P., Nohl, U., Herwig, K., Lammel, E., Stoll, B., & Hofmann, A. W. (2005). GeoReM: A new geochemical database for reference materials and isotopic standards. *Geostandards and Geoanalytical Research*, *29*(3), 333–338. https://doi.org/10.1111/j.1751-908X.2005.tb00904.x

Weiss, R. F. (1971). Solubility of helium and neon in water and seawater. *Journal of Chemical & Engineering Data*, *16*(2), 235–241. https://doi.org/10.1021/je60049a019